iScience

Article

OAS1 and *OAS3* genetic variants enhance inflammatory responses to SARS-CoV-2

Graphical abstract

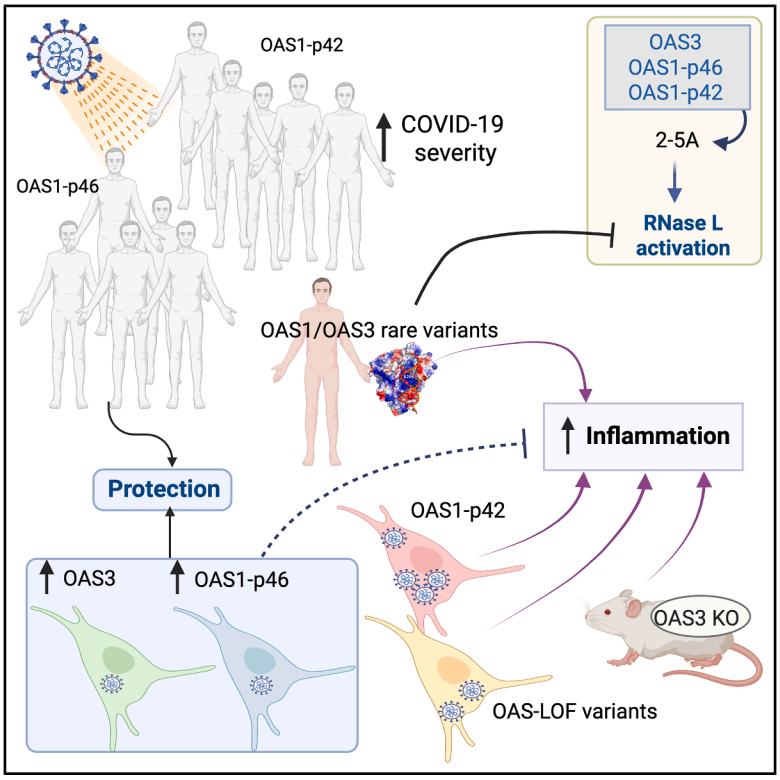

Highlights

- Rare OAS1/OAS3 variants in heterozygosity are not linked to severe COVID-19 hypoxemia
- Common OAS1 rs10774671 A/A genotype is linked to higher COVID-19 severity
- OAS system reveals mechanistic split between antiviral defense and inflammation
- Impaired RNase L activation may promote inflammation after SARS-CoV-2 infection

Authors

Marta L. DeDiego, Raúl López-Fernández-Sobrino, Jordi Pedragosa, ..., Israel Fernández-Cadenas, Jordi Pérez-Tur, Anna M. Planas

Correspondence

marta.lopez@cnb.csic.es (M.L.D.), jpereztur@ibv.csic.es (J.P.-T.), anna.planas@iibb.csic.es (A.M.P.)

In brief

Genetics; Immunology

DeDiego et al., 2025, iScience *28*, 113966
December 19, 2025
https://doi.org/10.1016/j.isci.2025.113966

CellPress

iScience

CellPress
OPEN ACCESS

Article

OAS1 and *OAS3* genetic variants enhance inflammatory responses to SARS-CoV-2

Marta L. DeDiego,[1,*] Raúl López-Fernández-Sobrino,[1] Jordi Pedragosa,[2,3] Darío López-García,[1] Aitor Nogales,[4] Jordi Durbán,[5] Fernando Cardona,[5,6] Laia Llucià-Carol,[2,7] Vanessa Rivero,[1] Paula Vazquez-Utrilla,[1] Laura Palomo Sanchez-Grande,[1] Miriam Cobo,[8] Lara Lloret,[8] Leonardo Márquez-Kisinousky,[2] Francisca Ruiz-Jaén,[2,3] Francisco Lozano,[3,9] Oriol Sibila,[3,9,10] Rosa Faner,[3,10] Pedro Castro,[3,9] Carlos Domingo,[9] Verónica Robles,[9] Josep L. Bedini,[9] Verónica Rico,[9] Daiana Aguero,[9] Alex Soriano,[3,9] Andrea Martín Nalda,[11]

(Author list continued on next page)

[1]Department of Molecular and Cell Biology, National Center for Biotechnology (CNB-CSIC), Campus Universidad Autónoma de Madrid, Madrid, Spain
[2]Department of Neuroscience and Experimental Therapeutics, Institute for Biomedical Research of Barcelona (IIBB-CSIC), Barcelona, Spain
[3]Institut d'Investigacions Biomèdiques August Pi i Sunyer (IDIBAPS), Barcelona, Spain
[4]Center for Animal Health Research (CISA-INIA-CSIC), Madrid, Valdeolmos, Spain
[5]Institute of Biomedicine of Valencia (IBV-CSIC), València, Spain
[6]CIBERNED, ISCIII, València, Spain
[7]Stroke Pharmacogenomics and Genetics, Institut de Recerca Sant Pau (IR SANT PAU), Barcelona, Spain
[8]Instituto de Física de Cantabria (IFCA-CSIC), Santander, Spain
[9]Hospital Clínic de Barcelona, Barcelona, Spain
[10]CIBER Enfermedades Respiratorias (CIBERES), Instituto de Salud Carlos III (ISCIII), Madrid, Spain
[11]Pediatric Infectious Diseases and Immunodeficiencies Unit, Hospital Universitari Vall d'Hebron, Vall d'Hebron Research Institute (VHIR), Vall d'Hebron Barcelona Hospital Campus, Universitat Autònoma de Barcelona (UAB), Barcelona, Catalonia, Spain
[12]Immunology Division, Department of Clinical and Molecular Genetics, Hospital Universitari Vall d'Hebron (HUVH), Vall d'Hebron Research Institute, UAB, Barcelona, Catalonia, Spain
[13]Hospital Universitari Mutua Terrassa, Terrasa, Spain
[14]Hospital Clínic de València, València, Spain
[15]Hospital General Universitari d'Alacant, Alacant, Spain
[16]Hospital Universitari i Politècnic 'La Fé', València, Spain
[17]Fundació per al Foment de la Investigació Sanitària i Biomèdica de la Comunitat Valenciana, València, Spain
[18]Mucosal Immunology Laboratory, Institute of Biomedicine and Molecular Genetics (IBGM), University of Valladolid-CSIC, Valladolid, Spain
[19]CIBERehd, ISCIII, Madrid, Spain
[20]Next Generation Sequencing Core Facility, German Cancer Research Center (DKFZ), Heidelberg, Germany

(Affiliations continued on next page)

SUMMARY

Recessive deficiency in 2′,5′-oligoadenylate synthetase (OAS) or RNase L can cause systemic inflammation in children with SARS-CoV-2 infection, but its role in adult respiratory disease is unclear. We analyzed rare *OAS1/OAS3* variants and the common *OAS1* rs10774671 polymorphism in 342 COVID-19 patients, assessing enzymatic activity, RNase L activation, viral replication, and inflammation in cell systems and *Oas3*-deficient mice. Rare heterozygous variants showed impaired RNase L activation but were not enriched in pneumonia cases. In contrast, the rs10774671 A/A genotype (OAS1-p42 isoform) was associated with severe disease (*OR* = 2.28; 95% CI = 1.13–4.58; p = 0.0107) and reduced viral control despite intact RNase L activation. OAS3 and OAS1-p46 isoform limited viral replication and inflammatory responses, whereas *Oas3*-deficient mice showed increased cytokines. These findings suggest that common *OAS1* variation influences COVID-19 severity, while rare *OAS* variants may affect inflammation regulation rather than respiratory pathology.

INTRODUCTION

Production of type I and III interferon (IFN) is known to be the first line of defense against viral infections. Accordingly, inborn errors of toll-like receptor (TLR) 3- and IFN-regulatory factor (IRF) 7-dependent type I IFN immunity have been identified as causally involved in life-threatening COVID-19 pneumonia in adults.[1,2] Several studies reported that loss-of-function (LOF)

Alba Parra Martínez,[11] Roger Colobran,[12] Pere Soler-Palacín,[11] Alexandre Serra-Llovich,[13] Beatriz Dietl,[13] M. Jesús Arranz,[13] David Dalmau,[13] Jaime Signes-Costa,[14] Joan Gil-Carbonell,[15] José Todolí,[16] Jacobo Martínez,[17] Silvia Rojo,[18] Aida Fiz-López,[18] Elisa Arribas,[18] Paloma Cal-Sabater,[18] David Bernado,[18,19] Marina Vogel,[20,21] Stefan Wiemann,[21] Hassan Abolhassani,[22] Qiang Pan-Hammarström,[22] Aurora Pujol,[23,24,25] COVID Human Genetic Effort[33], Helen C. Su,[26,27] Danyel Lee,[28,29,30] Shen-Ying Zhang,[28,29,30] Jean-Laurent Casanova,[28,29,30,31,32] Israel Fernández-Cadenas,[7] Jordi Pérez-Tur,[5,6,*] and Anna M. Planas[2,3,34,*]

[21]Division of Molecular Genome Analysis. German Cancer Research Center (DKFZ), Heidelberg, Germany
[22]Division of Immunology, Department of Medical Biochemistry & Biophysics, Karolinska Institutet, Solna, Sweden
[23]Neurometabolic Diseases Laboratory, Bellvitge Biomedical Research Institute (IDIBELL), L'Hospitalet de Llobregat, Barcelona, Spain
[24]Catalan Institution of Research and Advanced Studies (ICREA), Barcelona, Spain
[25]Center for Biomedical Research on Rare Diseases (CIBERER), ISCIII, Barcelona, Spain
[26]Laboratory of Clinical Immunology and Microbiology, Division of Intramural Research, NIAID, NIH, Bethesda, MD, USA
[27]Department of Pathology and Laboratory Medicine, Perelman School of Medicine, University of Pennsylvania, Philadelphia, PA, USA
[28]St. Giles Laboratory of Human Genetics of Infectious Diseases, Rockefeller Branch, The Rockefeller University, New York, NY, USA
[29]Laboratory of Human Genetics of Infectious Diseases, Necker Branch, INSERM U1163, Paris, France
[30]Paris City University, Imagine Institute, Paris, France
[31]Department of Pediatrics, Necker Hospital for Sick Children, Paris, France
[32]Howard Hughes Medical Institute, The Rockefeller University, New York, NY, USA
[33]Further details can be found in the supplemental information
[34]Lead contact
*Correspondence: marta.lopez@cnb.csic.es (M.L.D.), jpereztur@ibv.csic.es (J.P.-T.), anna.planas@iibb.csic.es (A.M.P.)
https://doi.org/10.1016/j.isci.2025.113966

variants in the *TLR7* gene are more prevalent in severely affected male patients.[3] Additionally, deficiency in *TLR7* compromises plasmacytoid dendritic cell sensing of SARS-CoV-2, thereby exacerbating the severity of COVID-19.[3–7] X-linked recessive *TLR7* deficiency and autosomal recessive *IFNAR1*, *STAT2*, or *TYK2* deficiencies were found in children with COVID-19 pneumonia.[8] Moreover, type I IFN auto-antibodies, which are highly prevalent in the elderly, hinder an efficient immune response against the viral infection and are an important risk factor for severe COVID-19 pneumonia at any age.[9–11] Type I IFNs induce a transcriptional program mediated by IFN-stimulated genes (ISGs) that trigger a powerful response.[12] This response is needed immediately after infection, and its strict regulation is of paramount importance. Delayed, prolonged, or deregulated type-I IFN responses may worsen viral or bacterial infections and promote autoimmunity,[13,14] and they could exacerbate the progression of SARS-CoV-2-triggered hyperinflammation, at least in children who did not develop COVID-19 pneumonia.[15] Severe adult COVID-19 patients showed a higher hyperinflammation in the blood, characterized by elevated levels of C-reactive protein (CRP) and interleukin-6 (IL-6).[16–19]

SARS-CoV-2 is a single-stranded RNA (ssRNA) virus that, like other coronaviruses, generates double-stranded RNA (dsRNA) early in the infection cycle due to genome replication and mRNA transcription.[20] The host cells recognize the presence of intracellular dsRNA by means of several sensors.[21,22] 2′,5′-oligoadenylate (2-5A) synthetase (OAS) proteins 1–3 are part of a largely conserved and complex dsRNA sensor and effector system mediated by the generation of 2-5A from ATP.[23] In turn, 2-5A activates the latent form of ribonuclease L (RNase L) that cleaves ssRNA from viral and host origin.[24–26] Upon RNA cleavage, RNase L generates small RNAs that can be recognized by retinoic acid-inducible gene I (RIG-I) and melanoma-differentiation-associated gene 5 (MDA-5), which could further enhance innate immune responses, including transcriptional induction of pro-inflammatory genes.[27] On the other hand, RNase L can degrade host RNA, including mRNA, rRNA, tRNA, and miRNA, thereby impairing global protein synthesis and preventing the expression of certain inducible proteins.[28–30] However, it selectively spares specific antiviral mRNAs, like IFN-β.[31] Expression of OAS1-3 is cell type specific, being most prominent in myeloid cells such as macrophages, and it can be boosted by the production of type I IFN since OAS1-3 are ISGs.[32]

A large genome-wide association study (GWAS) of COVID-19 patients identified genetic *loci* associated with disease severity with a small effect size.[33–35] One such *locus* is found in chromosome 12 and contains the *OAS1-3* gene family. Within this *locus*, the functional single nucleotide variant (SNV) rs10774671 was found to be associated with severe COVID-19.[33–36] This SNV controls the splicing and generation of two isoforms of OAS1, p46 and p42, corresponding to the G and the A alleles, respectively.[37] Interestingly, the G allele in rs10774671 is enriched in the European population and derives from an ancestral haplotype of Neanderthal origin.[38,39] Moreover, the G allele of *OAS1* encodes a prenylated more active form of the enzyme.[40] This *OAS1* splice variant is associated with a slightly reduced risk of becoming critically ill after SARS-CoV-2 infection.[36,41] A recent study showed that rs10776471 participates in the formation of a risk haplotype for COVID-19 severity by decreasing OAS1 protein expression through allele-specific regulation of splicing and nonsense-mediated decay.[42] Notably, inborn errors in the OAS-RNase L pathway were identified among children with multisystem inflammatory syndrome (MIS-C) associated with SARS-CoV-2 infection.[43] Patients with MIS-C commonly did not exhibit COVID-19 pneumonia, including the patients with OAS-RNase L genetic defects, attesting to the redundancy of the OAS-RNase L pathway for protective immunity against SARS-CoV-2 in the respiratory tract. We tested in cellular and animal models the hypothesis that rare variants in this pathway may impair the response to SARS-CoV-2 infection, by affecting viral replication and/or inflammation.

Table 1. Demographical and clinical summary of the Spanish population analyzed in this study

	Total	Hospitalized ICU	Hospitalized non ICU	Non Hospitalized
N	342	61	199	82
Sex (female N(%))	159 (46.6%)	17 (27.9%)	82 (41.4%)	60 (73.2%)
Age (SD; range)	46.9 (11.4; 18–65)	52.1 (9.3; 28–62)	45.3 (10.7; 22–65)	46.9 (13.1; 18–64)
Age women (SD; range)	46.5 (11.9; 18–65)	51.1 (11.1; 28–62)	45.5 (11.4; 22–65)	46.6 (12.8; 18–64)
Age men (SD; range)	47.1 (10.9; 20–64)	52.4 (8.7; 31–64)	45.0 (10.3; 23–64)	47.6 (14.2; 20–64)
Ancestry[a]				
EUR	212	42	92	78
AMR	113	15	95	3
OTHER	17	4	12	1

SD, standard deviation; ICU, Intensive care unit.
[a]EUR: Caucasian; AMR: Admixed American; OTHER:Other ancestries, combining East Asian, South Asian and African.

RESULTS

Clinical and epidemiological characteristics of the population under study

COVID-19 patients (n = 342) were aged 18–65 years and free of major chronic or acute diseases (see exclusion criteria in STAR Methods section). The demographic and hospitalization information on the individuals analyzed in this study is shown in Table 1. As expected,[44,45] men were more prone to show severe clinical characteristics than women. Within each clinical group, there were no differences in age between the two sexes (Table 1).

Genetic variants identified in a Spanish cohort of COVID-19 cases

We focused on the genetic variability in *OAS1*, *OAS2,* and *OAS3* due to previous reports on the role of this locus in SARS-CoV-2 infection and severity, and the strong linkage disequilibrium existing among them.[35] Table 2 shows the different variants found in the Spanish cohort for *OAS1*, *OAS2*, and *OAS3*, together with the pathogenicity prediction using several bioinformatic tools. All rare (minor allele frequency (MAF) < 0.05) and ultra-rare (MAF<0.001) variants were found in a heterozygous state. We did not further analyze *OAS2* since no variants predicted to be pathogenic were found for this gene in our cohort (Table 2). We found more than one ultra-rare variant for *OAS1* or *OAS3* in three individuals. By cloning and sequencing of PCR fragments, we found a compound heterozygous patient who carried two ultra-rare OAS1 variants in one allele (E120D and R256Q) and the V135L variant in the other allele. Another two patients carried two variants in the same allele in OAS3: A584T and A722G in one case, and D277G and E499K in the other.

We searched for additional variants from whole exome- or whole genome-sequencing data of hospitalized patients infected with SARS-CoV-2 of the international CHGE cohort (https://www.covidhge.com/) (n = 5,385 SARS-CoV-2 infected patients; n = 3,686 critical patients and n = 1,699 non-critical patients; Data S1). The search was based on similar criteria, but selected those *OAS1* and *OAS3* missense variants located in protein domains in addition to variants selected in the Spanish cohort. We considered patients of the same age range as in our Spanish cohort (18–65 years). In the CHGE cohort, novel ultra-rare variants were found in a heterozygous state (V55M and R256P in *OAS1*, and R188Q, K207M, R767C, and R932W in *OAS3*) (Data S1).

Overall, 24 (n = 9 for *OAS1* and n = 15 for *OAS3*) variants were predicted to be potentially damaging by multiple *in silico* tools. For functional testing *in vitro* in cellular systems, we selected 28 variants (n = 9 for *OAS1* and n = 19 for *OAS3*) found in the Spanish and CHGE cohorts (Figure 1A and Data S2). Although most of these variants were ultra-rare, we included the rare variants, R65W, V456I, and R932Q found in *OAS3* based on the predicted structural effect (R65W and R932Q) or because the location at a position relevant to the enzymatic activity of *OAS3* (V456I). In addition, we included a common variant, A727S in *OAS3,* which is ultra-rare among Europeans but common among Latinos, or rare variants that appear in combination with other ultra-rare variants in the same allele. The A727S variant showed no predicted deleterious effects and was used as a control (i.e., neutral variant) in our study. An alignment of *OAS1* and the three catalytic OAS domains of *OAS3*, showing the position of all variants, is found in Figure S1.

In silico prediction of structural alterations in a missense variant

The analysis of the 28 ultra-rare and rare variants in *OAS1* and *OAS3* using structural homology allowed us to identify those most likely to introduce a significant alteration in the function of the protein, in addition to those variants identified by the *in-silico* prediction tools. Some of the most significant findings are summarized in Data S2 and Figure S2. Data S2 describes the OAS variants found in our cohort of COVID-19 patients, their frequency, the bioinformatic prediction of deleteriousness, when possible, the predicted structural alteration associated with each variant, and the reason for variant selection for further functional assays.

Clinical severity of COVID-19 patients of the Spanish cohort carriers of *OAS1* and *OAS3* heterozygous missense variants

We studied the clinical features of the COVID-19 patients from the Spanish cohort with *OAS1* or *OAS3* genetic variants. They

Table 2. List of OAS genetic variants found in the Spanish population with prediction of functional effect using different tools

Position	N[a]	Gene	Ref. allele	Alt. allele	Protein change	rsID[b]	ClinVar[b]	MAF[c] (EUR)	MAF[c] (LAT)	REVEL[d]	SIFT[e]	PolyPhen2[f]	CADD[g]	Mut. Taster[h]	Patients
113346520	1	*OAS1*	G	T	E120D	(rs2043333587)	–	New	N/A	0.025	T (0.07)	PrD (0.987)	16.13	P	P1
113346563	1	*OAS1*	G	C	V135L	(rs111902215)	(1962088)	New	N/A	0.040	T (0.09)	PoD (0.477)	7.19	P	P1
113348870	F	*OAS1*	G	A	G162S	rs1131454	29024	0.52540	0.69750	0.183	T (0.13)	B (0.011)	3.09	P	–
113348994	1	*OAS1*	C	T	T203I	(rs750099581)	–	New	N/A	0.287	D (0.03)	PoD (0.903)	23.20	P	P6
113349002	1	*OAS1*	A	C	K206Q	(rs1593155771)	–	New	N/A	0.425	D (0)	PrD (0.984)	23.40	P	P4
113354426	3	*OAS1*	G	A	R256Q	rs528923373	1482420	0.00000	0.00011	0.146	T (0.16)	PoD (0.703)	4.16	P	P1, P2, P3
113354534	1	*OAS1*	C	T	T292M	rs778367989	1449870	0.00000	0.00065	0.112	D (0.03)	PrD (0.976)	6.51	P	P5
113357442	F	*OAS1*	G	A	G397R	rs2660	–	0.62430	0.82550	0.234	N/A	B (0.075)	6.28	P	–
113376388	F	*OAS3*	G	T	R18K	rs1859330	–	0.61270	0.79260	0.106	T (0.2)	B (0.015)	7.42	P	–
113379385	1	*OAS3*	C	T	S63L	rs772855388	–	0.00000	0.00061	0.059	T (0.42)	B (0.273)	5.75	P	–
113379390	8	*OAS3*	C	T	R65W	rs12819767	–	0.01359	0.00998	0.183	D (0)	PrD (1)	24.20	P	P21-P28
113379478	1	*OAS3*	G	A	R94H	rs745545367	2481890	0.00009	0.00000	0.021	T (0.05)	B (0.029)	11.84	P	–
113382281	1	*OAS3*	G	T	G154V	rs200770928	–	0.00017	0.00025	0.247	D (0)	PrD (1)	29.80	DC	P11
113384669	1	*OAS3*	G	A	R253Q	rs764044255	–	0.00000	0.00000	0.085	T (0.18)	PrD (0.96)	20.30	P	P13
113384741	1	*OAS3*	A	G	D277G	rs183804250	–	0.00104	0.00006	0.216	D (0.02)	PoD (0.892)	23.70	P	P12
113386754	1	*OAS3*	A	G	N373S	rs769669888	2382510	0.00026	0.00009	0.007	T (0.46)	B (0)	0.002	P	–
113386769	1	*OAS3*	G	A	R378K	rs45519442	–	0.00009	0.00037	0.052	T (0.74)	B (0)	1.25	P	–
113386779	F	*OAS3*	C	G	S381R	rs2285933	–	0.26080	0.32720	0.073	TLC (0.55)	B (0.139)	0.81	P	–
113386888	1	*OAS3*	C	T	R418C	rs765652205	–	0.00009	0.00003	0.052	D (0.02)	B (0.05)	23.30	P	P16
113386889	1	*OAS3*	G	A	R418H	rs373103415	–	0.00061	0.00023	0.080	D (0.01)	PrD (0.994)	24.80	P	P8
113387002	2	*OAS3*	G	A	V456I	rs185547332	–	0.00167	0.00147	0.036	T (0.07)	B (0.182)	13.70	P	P29-P30
113388598	2	*OAS3*	G	A	R492H	rs115666428	702134	0.00368	0.00198	0.025	T (0.46)	B (0.007)	9.96	P	–
113388618	1	*OAS3*	G	A	E499K	rs199505039	–	0.00096	0.00006	0.068	T (0.19)	B (0.027)	16.86	P	P12
113388625	2	*OAS3*	G	A	R501Q	rs746297884	–	0.00000	0.00000	0.030	T (0.23)	B (0.05)	12.05	P	–
113398968	1	*OAS3*	G	A	A584T	rs35508906	–	0.00035	0.00045	0.006	T (1)	B (0.007)	0.08	P	P7
113398998	1	*OAS3*	C	T	R594C	rs776108063	–	0.00000	0.00000	0.064	D (0.04)	B (0.205)	20.40	P	P9
113399047	2	*OAS3*	G	A	R610H	rs779154930	–	0.00000	0.00009	0.042	T (0.26)	B (0.058)	0.63	P	–
113401198	1	*OAS3*	C	G	A722G	rs1018742530	–	0.00000	0.00004	0.051	T (0.12)	B (0.383)	5.30	P	P7
113401212	F	*OAS3*	G	T	A727S	rs45607836	–	0.00035	0.14870	0.015	T (0.39)	B (0.163)	5.42	P	–
113403628	1	*OAS3*	A	T	Q828L	rs756226307	–	0.00035	0.00034	0.045	D (0.02)	PoD (0.642)	16.70	P	P14
113405292	1	*OAS3*	C	T	A920V	rs539747098	–	0.00009	0.00009	0.085	T (0.13)	PrD (0.979)	16.08	P	P10
113405328	5	*OAS3*	G	A	R932Q	rs61732395	–	0.00784	0.00252	0.234	D (0.02)	PrD(1)	23.20	P	P17-P20
113405825	1	*OAS3*	G	A	G984R	rs374768377	–	0.00000	0.00003	0.106	D (0.04)	PrD (0.989)	18.38	P	P15

(*Continued on next page*)

Table 2. *Continued*

Position	N[a]	Gene	Ref. allele	Alt. allele	Protein change	rsID[b]	ClinVar[b]	MAF[c] (EUR)	MAF[c] (LAT)	REVEL[d]	SIFT[e]	PolyPhen2[f]	CADD[g]	Mut. Taster[h]	Patients
113407773	1	*OAS3*	G	A	V1087M	rs45620632	–	0.00116	0.00279	0.073	D (0)	PrD (0.971)	22.50	P	–
113440906	1	*OAS2*	G	A	R393Q	rs150642424	–	0.00000	0.00031	0.032	T (0.11)	B (0.001)	11.28	P	–
113445604	1	*OAS2*	C	T	P584L	rs984868313	–	0.00000	0.00000	0.011	T (0.28)	B (0.003)	0.002	P	–

Position, in the chromosome; N, number of carriers in the population; Ref, reference; Alt., Alternative; Protein change, amino acid variant; rsID, SNV reference number; ClinVar, ID reference in the ClinVar database.

[a]Number of individuals with the variant. F indicates high frequency (MAF>0.05) in at least one of the populations.

[b]Between brackets, ID of a variant in the same position but with a different change.

[c]Minor allele frequency according to gnom AD v2.1.1 for EUR (Non-Finnish Europeans) and LAT (Latino/Admixed American populations).

[d]REVEL score, >0.500 suggests pathogenicity.

[e]SIFT score, qualitative (quantitative) values. N/A: score not provided. T: tolerated; D: Deleterious; TLC: tolerated_low_confidence.

[f]PolyPhen2 score, qualitative (quantitative) values. PrD: Probably damaging; PoD: Possibly damaging; B: Benign.

[g]CADD, quantitative values. Arbitrary score >15 suggests pathogenicity.

[h]Mutation (Mut.) Taster qualitative values. P: polymorphism; DC: Disease-causing.

included 6 heterozygous variants that could be putatively pathogenic, found in *OAS1* in 6 patients, and 15 heterozygous variants in *OAS3* found in 24 additional patients. No patients were found to carry any potentially pathogenic variant simultaneously in both *OAS1* and *OAS3,* although 3 patients carried more than one single rare or ultra-rare variant in one of those two genes. Altogether, we report 30 patients with ultra-rare or rare OAS variants with *in silico* prediction indicating they could be pathogenic. Amongst them, 12 were women and 18 were men. Men required ICU-level care more frequently than women (5:2), and all hospitalized patients (non-ICU) showing moderate COVID-19 disease with strong inflammatory responses (n = 8) were men. Hospitalized patients with mild disease (n = 10) were 5 men and 5 women. Non-hospitalized patients were 5 women. Most of the patients (73%) had the A/A genotype for the rs10774671 OAS1 polymorphism, resulting in the expression of the OAS1-p42 isoform. The remaining patients carried the A/G alleles and therefore expressed both the p42 and p46 isoforms. The basic characteristics of COVID-19 patients carrying *OAS1* or *OAS3* ultra-rare heterozygous variants (patients P1-P16), and patients harboring rare (R) heterozygous *OAS3* variants (P17-P30) are summarized in Figure 2 (see details of the patients in the STAR Methods section).

Missense variants in the general population

Enrichment analysis in the Spanish cohort was made on the presence of variants in *OAS1* and *OAS3* individually or, because of their physical proximity, considering both genes as part of the same *locus* and combining variants from both genes together. No significant enrichment was observed under any of these analytical paradigms when considering the groups defined in this analysis (Hospitalized vs. Non-hospitalized), nor when considering the two most extreme phenotypes (individuals requiring ICU vs. non-hospitalized individuals, Table 3), although a trend was observed for OAS3 when comparing ICU patients versus non-hospitalized patients.

Genotype of the *OAS1* common variant rs10774671

Given the documented functional differences and clinical association with severity between the alternatively spliced isoforms OAS1 p42 (rs10774671 – A allele) and OAS1 p46 (rs10774671 – G allele) (37, 63), we studied the genotype for this common variant in patients of the Spanish cohort (Table 4; Figure 2). We observed a significant difference in the allelic distribution between all groups (Chi-square p = 0.0333; 2 df). This difference was associated with an increase in the frequency of the A allele in the hospitalized population. Moreover, the A/A genotype was significantly increased when comparing the two most extreme phenotypes in our cohort: patients requiring ICU admission vs. patients not requiring hospitalization. The OR for carrying this genotype was of 2.28 ($CI_{95\%}$ = [1.13–4.58], p = 0.0107). The association of the rs10774671 – A/A genotype with clinical severity in our population agrees with previous GWAS data.[33–36,41]

We also analyzed the genetic effect of the presence of the A allele in the enrichment of rare and ultrarare variants in our population. For this, we repeated the SKAT analysis, including the genotype at rs10774671 as a covariate under two different

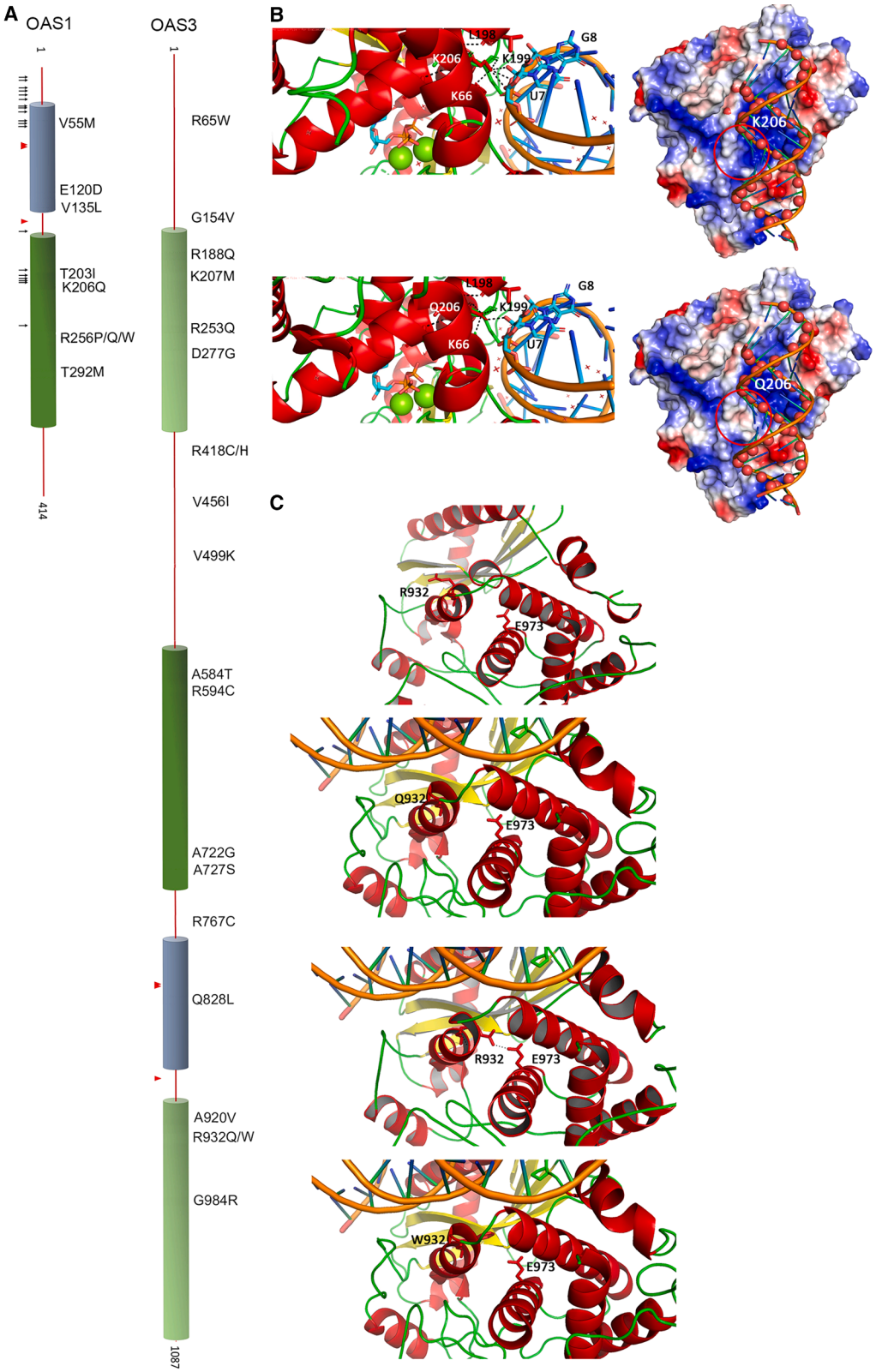

(legend on next page)

models, SKAT-O, equivalent to the one done without including the effect of rs10774671, and another SKAT method to study the combined effect of common and rare variants. None of these analyses revealed a significant enrichment of rare and ultrarare variants in the cohort (p = 0.8721 SKAT-O; p = 0.7128 SKAT-CommonRare).

Regression analysis

Our multivariate regression analysis confirmed, on the one hand, that age and sex are important predictors of severity ($p < 0.001$ in each case) with male and older age increasing the risk of a more severe form of COVID-19 and, on the other, that being of Latin-American ancestry slightly increased the risk of a more severe form of COVID-19 ($p < 0.05$). With no interaction of age and presence of rare variants (p = 0.681).

In the bivariate analysis, comparing non-hospitalized patients with those hospitalized regardless of ICU admission, the results were similar. The model obtained was highly significant ($p < 0.0001$) and explained nearly 25% of the variation in hospitalization outcome (pseudo-R-square = 0.2527). In this analysis, sex ($p < 0.001$) and ethnicity ($p < 0.05$) were significant predictors of severity. Again, male individuals and a Latin-American ancestry were associated with severity. Age was not significantly associated with severity in this analysis, although a trend was observed (p = 0.062), which may be due to the exclusion of patients older than 65 from the study. Both analyses showed that there was no association of the severity of COVID-19 infection with either rare variants found in the population or the genotype at the rs10774671.

Effect of *OAS1* variants on enzymatic activity

OAS1 and OAS3 are activated upon dsRNA binding, leading to the synthesis of 2-5A. Aiming to study the effect of the OAS genetic variants on the protein enzymatic activity, we generated OAS1 recombinant proteins. We also attempted to generate recombinant OAS3 but we did not succeed, likely due to the long length of this protein. Human recombinant WT OAS1-p42 was compared with human recombinant WT OAS1-p46. We also generated the OAS1-K206Q variant on the OAS1-p46 isoform as a representative of the variants located in RNA-binding domains and classified as potentially pathogenic through *in silico* predictions. We studied whether the genetic variants affected the capacity of the OAS enzyme to produce 2-5A from ATP. The different variant enzymes were titrated serially (2-fold) to determine the optimal concentration (Figure 3A). Enzyme reactions containing ATP and dsRNA were used to determine the amount of 2-5A formed. The K206Q OAS1-p46 variant had a much higher EC50 and generated significantly less 2-5A than the WT isoforms (Figures 3A and 3B). The enzyme-specific activity (measured in 2-5A μmol/min/mg) was dramatically lower for K206Q OAS1-p46 (35.5) compared to WT OAS1-p46 (82,687.9) and WT OAS1-p42 (35,911.2). Moreover, a comparison of the WT p46 and WT p42 isoforms revealed that the specific activity of WT OAS1-p46 *in vitro* was 2.3 times higher, resulting in a higher production of 2-5A than the WT OAS1-p42 isoform, in agreement with a previous report (34). Although the common isoform p42 has slightly lower enzymatic activity than p46, this reduction is much smaller in magnitude compared to the effect of the K206Q variant. Defective production of 2-5A by the K206Q variant is likely due to defective dsRNA recognition, as this residue is located in a region involved in dsRNA binding (Figure 1A). Since OAS1-mediated 2-5A synthesis activates endonuclease RNase L (24,26), the K206Q variant is expected to impair RNase L activation.

Effect of *OAS1* and *OAS3* variants on RNase L activation and viral load

We examined whether the *OAS1* and *OAS3* variants identified in SARS-CoV-2 infected patients can affect the function of the proteins with respect to RNase L activation as they may reduce enzymatic activity. First, we evaluated potential differences in RNase L activation between the p42 and p46 *OAS1* isoforms in HEK293T-ACE2 cells, which naturally express the SNV rs10774671(A/A) genotype corresponding to OAS1-p42 protein, and therefore lack OAS1-p46 expression. Transfection of these cells with plasmids expressing either the A or G alleles induced the expression of similar levels of OAS1-p42 and OAS1-p46, as assessed by Western blotting 24- and 48-h post-transfection (hpt) (Figure S3A). The integrity of the rRNAs was measured as an indirect assessment of RNase L activity in mock-transfected and poly(I:C)-transfected cells. Poly(I:C) is a synthetic dsRNA that induces the expression of OAS proteins, causing RNase L activation.[29] No differences were observed in poly(I:C)-induced rRNA degradation between OAS1 p42-and p46-overexpressing cells (Figure S3B). Consequently, the small differences in the enzymatic capacity between p42 and p46 observed *in vitro*

Figure 1. Position and predicted effect of the variants found in this study

(A) Schematic representation of OAS1 and OAS3. In blue, the nucleotidyl-transferase domain. In green, the OAS domains with catalytic domains are shown in darker green. Red arrowheads point to the location of the Asp residues involved in the catalytic center. Black arrows in OAS1 point to the residues involved in dsRNA binding.

(B) Modeling of the effect of the OAS1 K206Q variant in a 3D structural model of the protein (top part of the panel) and in the superficial electrical charge (bottom part of the panel). This variant modifies the hydrogen bridges formed by the WT residue, weakening the interaction at this area and provoking a significant change in the electrostatic surface of the protein (bottom part of the panel). In the representation of the electrostatic charge at the surface of OAS1, shown in the bottom part of panel 1B, in blue color we represent positive charges, red represents a negative environment, whereas white indicates non-charged areas.

(C) Effect of variants at the OAS3 R932 position. The top part of the panel shows the structural change produced by the binding of a dsRNA molecule to the third OAS domain in WT (R932) OAS3. If no RNA is bound (left image in top panel), OAS3 remains inactive. The binding of a dsRNA molecule (right image of the top panel, dsRNA depicted in brown with blue sticks representing the nucleotide pairs) prompts a structural change that places R932 in the vicinity of E973, creating some hydrogen bonds and promoting a change in the structural conformation of the active center that allows the synthesis of the 2-5A. The two variants, Q932 and W932 (bottom part of the panel), are unable to form hydrogen bonds with the E973 residue and, therefore, the active center of the protein is not able to efficiently promote the synthesis of 2-5A. In the 3D protein representations, the red ribbons represent the parts of the protein ordered as an α-helix, yellow arrows represent parts folded as a β-sheet and unstructured regions are shown in green. See Figures S1 and S2 for additional information.

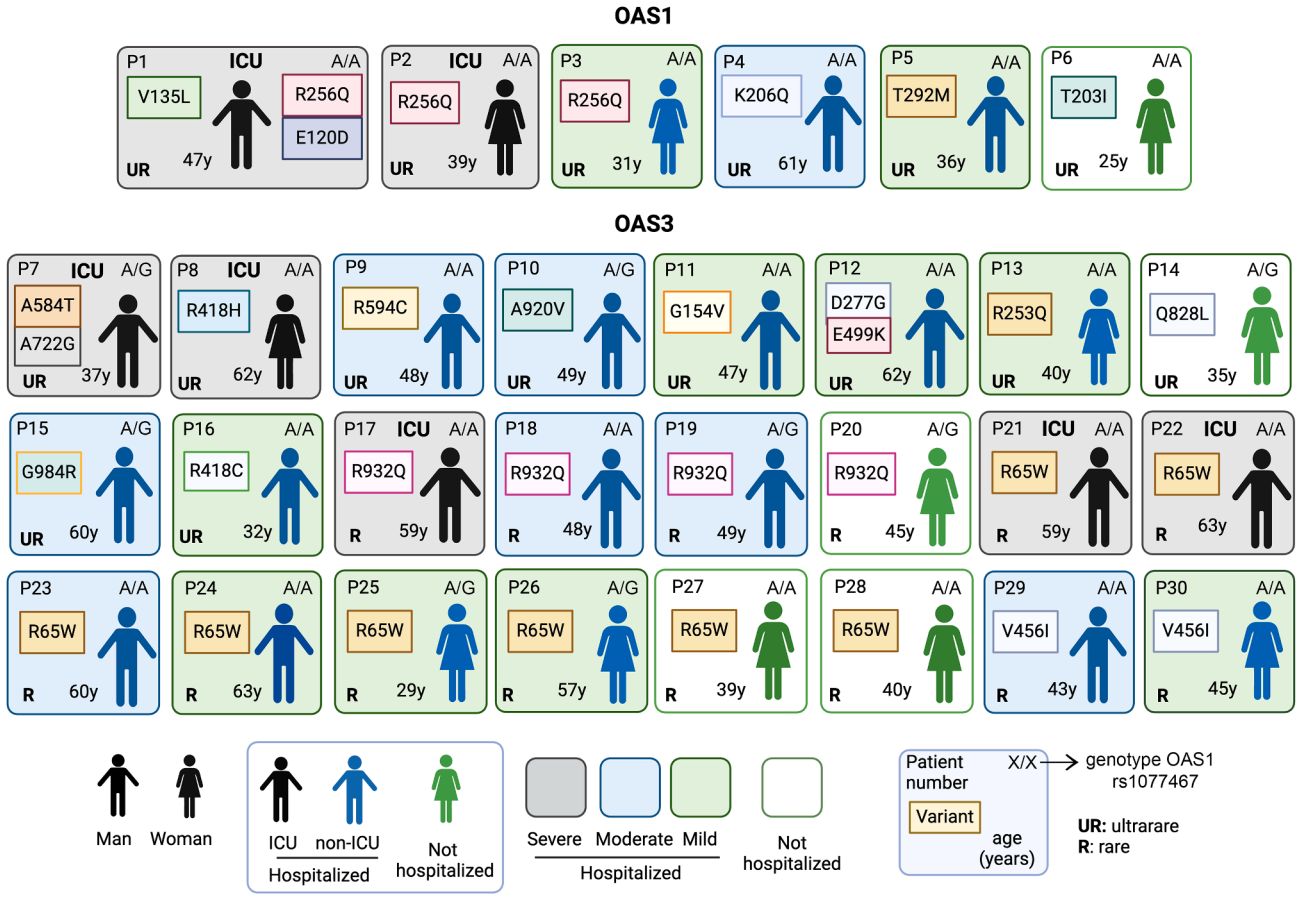

Figure 2. Summary of OAS1 and OAS3 ultra-rare and rare missense variants found in patients of the Spanish cohort of COVID-19 patients

Variants are ultra-rare (UR) or rare (R). Black human figure/gray background indicates hospitalization in the intensive care unit (ICU) due to severe/critical disease. Blue human figure indicates hospitalization (not ICU), with either blue background indicating moderate disease accompanied by a strong inflammatory reaction (e.g., high CRP and ferritin), or green background indicating mild disease devoid of inflammatory biochemical parameters in serum. Green human figure/white background indicates non-hospitalized. Px is the number assigned to each patient for data presentation (see Material and STAR Methods section for a clinical description). The genotype of the OAS1 polymorphism (rs1077467) is shown in the top right corner of each individual square; age is indicated (y, years) in the bottom, and sex is represented by standard man and woman figures. Further details of the clinical course and inflammatory indicators of these patients are described in the STAR Methods section.

(Figure 3) were not sufficient to cause noticeable variations in rRNA degradation under the current assay conditions. However, we cannot rule out the possibility that the degradation capacities of the isoforms may differ for other ssRNAs, or that the effects observed under conditions of isoform overexpression may not accurately reflect those under physiological conditions, where OAS expression levels may be different.

To investigate the impact of the rare *OAS1* and *OAS3* variants identified in COVID-19 patients on RNase L activity, we transfected HEK293T-ACE2 cells with plasmids encoding either the rare variants or the corresponding wild-type forms. For *OAS1*, the rare variants were generated on the rs10774671 G/G background, which encodes the common OAS1-p46 isoform. Corresponding protein expression was assessed by Western blotting at 48 hpt (Figures S3C and S3D). We analyzed rRNA degradation following treatment with poly(I:C). The *OAS1* variants K206Q, T203I, R256P, and R256W (Figure 4A), and the *OAS3* variants -R418C, R594C, R767C, R932Q, R932W, and A584T + A722G (found in the same allele in one patient) (Figure 4B) showed statistically significant reductions in their capacity to activate RNase L. These variants were clearly LOF concerning RNase L activation. In addition, the *OAS1* variant - R256Q-, and the *OAS3* variants -K207M, R418H, and A920V- showed a trend to decrease rRNA degradation. We next examined whether the effect could also be reproduced in the *OAS1* rs10774671(A/A) genotype following transfection of HEK293T-ACE2 cells. Cells were treated with poly(I:C), and RNase L-mediated rRNA degradation was analyzed as above. As observed in the *OAS1* rs10774671(G/G) genotype (p46 isoform), the K206Q, R256W, and T203I *OAS1* rare variants on the rs10774671(A/A) genotype (p42 isoform) showed impaired RNase L activation (Figure S4A). In addition, none of the amino acid changes appeared to reduce OAS1-p42 protein expression (Figure S4B), as observed for the OAS1-p46 isoform.

We next studied whether the defective activation of RNase L by several *OAS1* and *OAS3* variants also occurred in

Table 3. Enrichment analysis of OAS1, OAS3 and OAS1 + OAS3 in the Spanish cohort

Comparison	*OAS1*	*OAS3*	*OAS1 + OAS3*
Hospitalized vs. non-hospitalized	0.264	0.142	0.110
ICU vs. Non-hospitalized	0.566	0.067	0.099

p-value of the SKAT-O association analysis for gene enrichment.

SARS-CoV-2-infected cultured cells. First, we overexpressed ACE2 in epithelial HEK-293T cells to enable SARS-CoV-2 cell infection. Then, HEK293T-ACE2 cells overexpressing *OAS1* rs10774671 (A/G) (V55M, K206Q, R256W) or *OAS3* (V456I, R932W) variants by means of plasmids, were infected with SARS-CoV-2. Again, K206Q and R256W *OAS1* and R932W *OAS3* variants caused defective RNase L activation (Figure 4C). These results show that certain mutations in *OAS1* and *OAS3* impair the capacity of the cells to activate RNase L following SARS-CoV-2 infection. Impaired RNase L activation is expected to reduce the degradation of viral RNA and also host RNA, which may weaken the inhibition of protein synthesis induced by viral infection.

Effects of loss or gain of function of OAS1 and OAS3 on RNase L activity and viral replication

We undertook loss- and gain-of-function experiments in cell cultures to explore whether the effect of OAS1 and OAS3 on RNase L activity would impact viral replication. First, we overexpressed ACE2 in epithelial A549 cells (A549-ACE2) to enable SARS-CoV-2 cell infection. A549 cells have the *OAS1* rs10774671(A/A) common genotype, thus basally expressing the OAS1-p42 isoform.[42] Following SARS-CoV-2 infection (MOI 1), A549-ACE2 cells showed degradation of rRNAs, which was more pronounced at 24 h post-infection (hpi) compared to 48 hpi (Figure 5A). Silencing *OAS3*, and to a lesser extent *OAS1*, in A549-ACE cells reduced RNase L activation induced by SARS-CoV-2 (Figure 5B). Moreover, silencing *OAS3*, but not *OAS1*, increased the viral titers (Figure 5C). Similarly to our results, previous studies highlighted a more prominent role for OAS3 over OAS1 in RNase L activation.[46–48] However, the lack of effect of *OAS1* silencing on RNase L activation and viral load observed in previous studies[46,48] and in our work may be due, at least in part, to the specific expression of OAS1-p42 in human A549 cells. An additional contributing factor could be the low endogenous expression of OAS1-p42 in A549 cells, even after poly(I:C) treatment, compared to the high expression of this protein when overexpressed it in 293T cells by means of a plasmid (Figure S4C). Therefore, the effect of OAS1 on RNase L activation and on antiviral activity may depend on the isoform expressed and the expression levels, which vary among different cells and tissues. We further analyzed the effect of OAS3 on RNase L activation by knocking down *OAS3* in A549-ACE2 cells using CRISPR/CAS9 technology. Two *OAS3* knockout (KO) clones were selected for our studies (Figure 5D). rRNA degradation was highly impaired in the *OAS3* KO cells treated with poly(I:C) versus the parental cells (Figure 5E). Moreover, rRNA integrity was preserved in *OAS3* KO cells after SARS-CoV-2 infection, in contrast to the compromised rRNA integrity in WT cells (Figure 5F). In agreement with the siRNA results (Figure 5C), viral titers in the cell culture supernatants increased 3 to 4-fold in the A549 *OAS3* KO cells compared to the parental control cells at 48 hpi (Figure 5G), indicating that OAS3 has a weak antiviral activity against SARS-CoV-2 in this cell line.

Previous studies have shown that overexpression of OAS1[40,49] and, to a much lower extent, OAS3[49] can decrease SARS-CoV-2 replication in A549-ACE2 lung epithelial cells in the absence of exogenous type I IFN treatment. To further analyze whether OAS1 and OAS3 restrict SARS-CoV-2 replication, HEK293T-ACE2 cells were transfected with plasmids to overexpress either OAS1-p46, OAS1-p42, or OAS3 (Figure 5H). Viral titers at 24 hpi were reduced in cells overexpressing OAS1-p46 or OAS3, while the effect of OAS1-p42 overexpression was comparatively poorer (Figure 5I). This result was replicated in A549-ACE2-*OAS3* KO cells overexpressing the various OAS proteins (Figure 5J). These results agree with previous studies showing that overexpression of OAS1-p46,[40,42,49,50] or OAS3[49] restricts SARS-CoV-2 replication, whereas OAS1-p42 overexpression does not.[50] Therefore, OAS1 p42 appeared unable to effectively restrict viral infection, despite showing RNase L activity degrading rRNA. The impaired ability of OAS1-p42 to inhibit viral replication may be attributed to differences in cellular localization between p42 and p46. Unlike p42, p46 undergoes post-translational prenylation, allowing it to anchor to cell membranes and access endosomal membranes, where viral replication occurs.[40,51] Thus, the mislocalization of p42 compared to p46 may explain its reduced effectiveness in

Table 4. Genotypic and allelic distributions of rs10774671 in the different groups of the Spanish cohort

	Genotypes[a]			Alleles[b]	
	A/A	A/G	G/G	A	G
Hosp. ICU	43 (70,49%)	17 (27,87%)	1 (1.64%)	103 (84,43%)	19 (15,57%)
Hosp. non ICU	36 (60,00%)	18 (30,00%)	6 (10,00%)	90 (75,00%)	30 (25,00%)
Non hosp.	42 (51,22%)	33 (40,24%)	7 (8.54%)	117 (71,34%)	47 (28,66%)

Hosp ICU: patients hospitalized requiring ICU admission. Hosp. non ICU: patients requiring hospital admission without needing ICU. Non hosp.: patients not requiring hospitalization.

In each cell the number of cases for each genotype or allele are shown together with their relative proportion (between brackets).

[a]ICU vs. non hosp. Fisher's exact test $p = 0.042$, 2df, OR = 2.28, CI_{95} = [1.13–4.58] $p = 0.011$. Hosp vs. non hosp.: Chi-square test, 1 df, $p = 0.045$; OR = 1.79; CI_{95} = [1.01–3.18], $p = 0.023$.

[b]ICU vs. non hosp: Chi-square test $p = 0.009$, 1df, OR = 2.18, CI_{95} = [1.20–3.95], $p = 0.0052$.

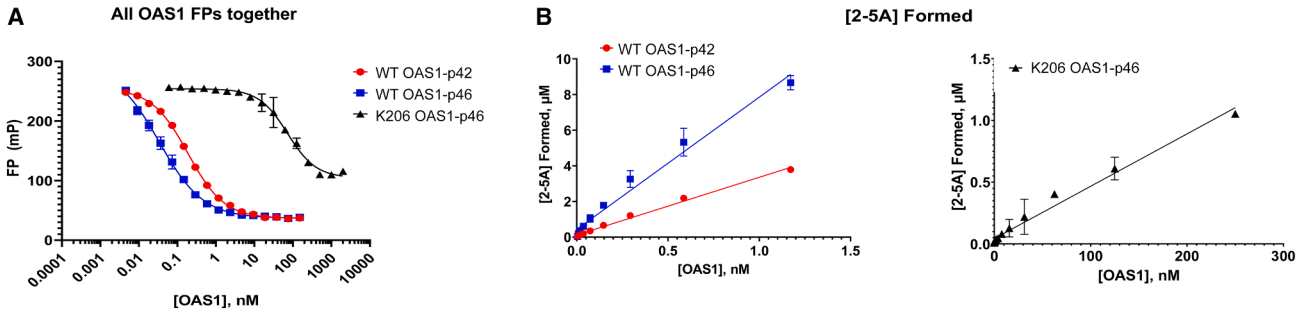

Figure 3. Enzymatic activity of WT OAS1-p42, WT OAS1-p46, and K206Q OAS1-p46

(A and B) Enzyme titrations. FP: Fluorescent Polarization. Data are represented as mean ± SD.

inhibiting viral infection, despite it can induce the degradation of host cytoplasmic RNA.

Effect of OAS1 and OAS3 on the induction of inflammatory responses

Given that potent inflammatory responses induced by SARS-CoV-2 are related to disease severity,[16,17,19] we investigated the potential impact of OAS1 and OAS3 on the expression of proinflammatory cytokine mRNAs. Once activated by 2-5A generated by OAS proteins, RNase L degrades viral and host RNA.[28–30] We studied the effect of downregulating *OAS1* rs10774671 (A/A) or *OAS3* mRNA expression in A549-ACE2 cells by more than 90% with siRNAs (as shown in Figure 5B). Silencing *OAS3* increased *IFNL1, TNF,* and *CXCL10* mRNA expression induced by poly(I:C) (Figure 6A), whereas the effect was less pronounced after silencing *OAS1* rs10774671 (A/A). The OAS3 effect was validated in two clones of *OAS3* KO cells (Figure 6B). We then tested the effect of infection with SARS-CoV-2 in cells with silenced *OAS1* rs10774671 (A/A) or *OAS3.* Again, we found that the reduction of OAS3 exacerbated the expression of *IFNL1* and *TNF* mRNA, compared to the control cells transfected with a control siRNA, while the effect of OAS1 p42 was negligible (Figure 6C). Therefore, OAS3 likely reduces pro-inflammatory cytokine mRNA by promoting RNase L-mediated host mRNA degradation, whereas OAS1-p42 has a milder effect, possibly due to reduced viral sensing and subsequent weaker RNase L activation.

To validate the observed effect of OAS3 and explore whether OAS1-p46 could affect the inflammatory response, we overexpressed these proteins (see Figure 5H). To this end, we transfected *OAS3* KO A549-ACE2 cells (clone 2) with *OAS1* (rs10774671, G/G) or *OAS3* plasmids. After confirming RNAse L activation following OAS1 and OAS3 overexpression (Figure S5), we analyzed mRNA expression of the pro-inflammatory genes. Overexpression of OAS1-p46 and OAS3 decreased the mRNA levels of *IFNL1, TNF, CCL2,* and *CXCL10* induced by poly(I:C), compared to the control cells transfected with an empty plasmid (Figure 6D). These results strongly suggest that OAS1-p46 and OAS3 exert an inhibitory control of inflammatory responses, possibly mediated by RNase L-dependent degradation of self mRNA, including viral induced pro-inflammatory cytokine mRNA.

To determine whether rare LOF variants in the OAS1 gene affect the inflammatory response, we overexpressed either OAS1-WT or the LOF variants OAS1-K206Q and OAS1-R256W, all on the background of the rs10774671 G/G polymorphism, in HEK293T-ACE2 cells. Overexpression of OAS1-p46 reduced the expression of pro-inflammatory mRNAs induced by poly(I:C); however, this effect was markedly impaired in the presence of the rare variants that disrupt RNase L activation (Figure 6E). These findings suggest that the anti-inflammatory effect of OAS1-p46 depends on RNase L, likely through the degradation of host mRNA. Additionally, we cannot exclude the possibility that certain non-canonical functions of OAS1 may be partially preserved in some LOF variants that fail to activate RNase L.

Inflammatory response of PBMCs to SARS-CoV-2 infection

To analyze whether cells from subjects encoding *OAS1* or *OAS3* variants could display exacerbated inflammatory responses, we obtained blood from 7 subjects of the Spanish cohort who were previously hospitalized due to COVID-19. Samples were obtained at least 18 months after recovery from COVID-19 (Figure 7A). We could obtain blood of two of the previous patients that were heterozygous carriers of ultra-rare *OAS1* or *OAS3* variants LOF for RNase L activation (P4 and P7 patients in Table 2; Figure 2). Both patients were hospitalized due to COVID-19, but only P7 (sample S2) had to be admitted to the ICU. P7 (PBMC sample S2) carried the A584T and A722G variants in *OAS3,* and P4 (PBMC sample S7) carried the *OAS1* K206Q variant, both causing LOF for RNase L activation (Figure 4). We also included four patients with non-pathogenic variants, and one patient (control) devoid of any OAS rare variant. Notably, sample S7 (P4) and sample S4 carried the A/A genotype for *OAS1* rs10774671 encoding OAS1-p42, whereas the remaining samples were heterozygous A/G for this polymorphism (Figure 7A).

PBMCs were either transfected with 2.5 µg/mL of poly(I:C) or infected (MOI 0.5) with SARS-CoV-2 for 24 h. To ensure that the *ex vivo* infection of PBMCs with SARS-CoV-2 was successful, we determined the levels of viral genomic RNA and subgenomic mRNAs (gene 7 sgmRNA) in the cells by RT-qPCR (Figure S6A), indicating that SARS-CoV-2 had successfully infected the PBMCs. The expression of *CCL2*, *CXCL10*, *TNF, IL-6* mRNA (Figures 7B–7D), and *OAS1, OAS2,* and *OAS3* mRNA (Figure S6B) was analyzed by RT-qPCR. No induction

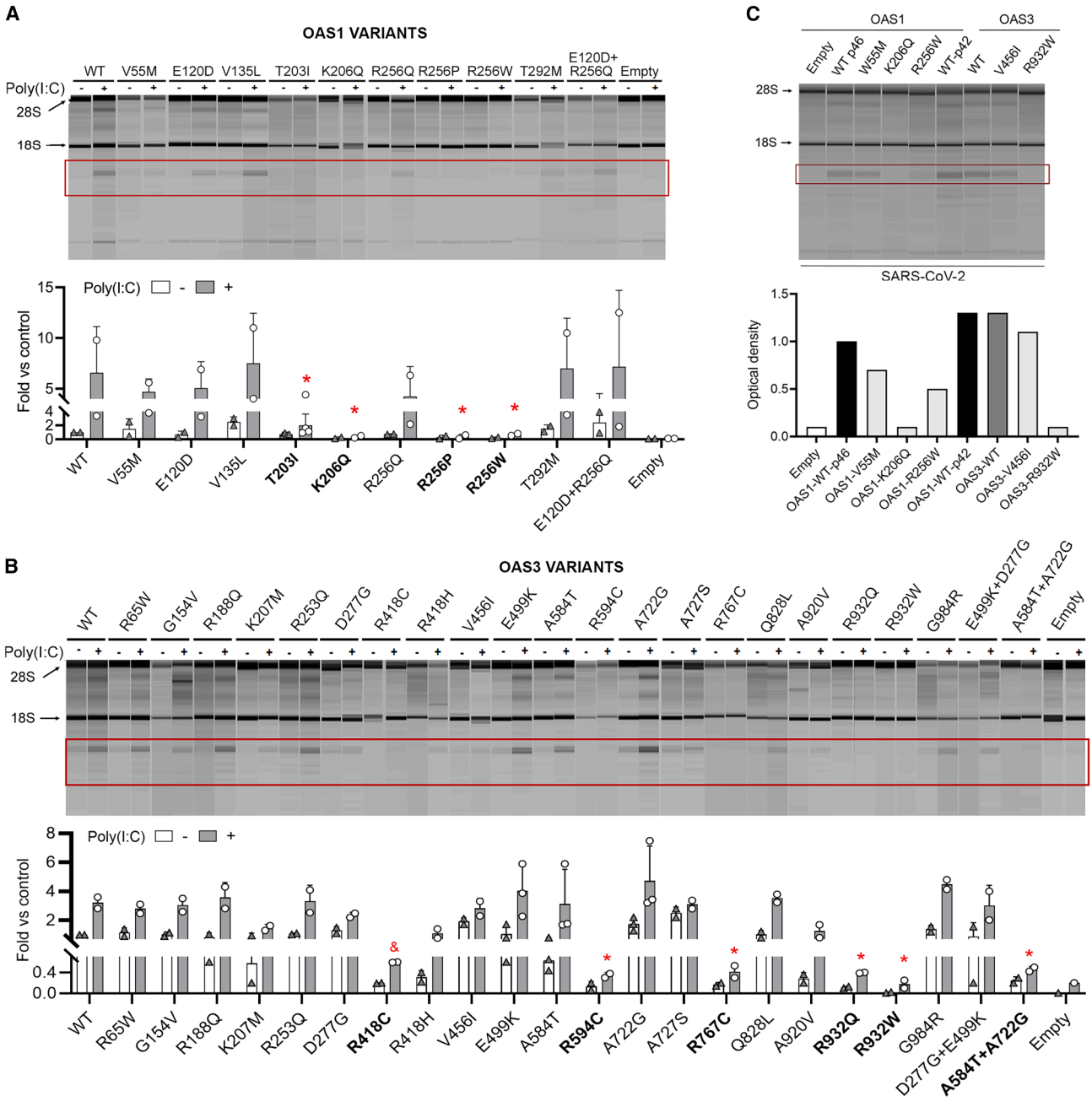

Figure 4. Effect of *OAS1* and *OAS3* variants on RNase L activation

HEK293T-ACE2 cells were transfected with plasmids expressing *OAS1* (A) and *OAS3* (B) WT and rare variant genes. For *OAS1*, we used the rs10774671 (G/G) common genotype. 'Empty' denotes transfection with an empty vector. At 24 hpt, the cells were left mock-transfected or transfected with poly(I:C). Total RNA was purified 24 h after poly(I:C) transfection and was analyzed in a Bioanalyzer. The amount of RNA degradation (red rectangle) was quantified by densitometry and normalized to the amount of the 18S rRNA (shown with an arrow on the left) within each sample. Densitometry values were normalized to the values in mock-treated cells transfected with the *OAS1*-WT (encoding OAS1-p46) (A) or *OAS3*-WT (B) plasmids. two-way ANOVA and Dunnett's multiple comparisons (n = 2–3 per variant). Red symbols denote significant differences vs. WT (names in bold) (for OAS1 variants: $^{*}p = 0.035$, $p = 0.015$, $p = 0.014$, and $p = 0.019$ corresponding to T203I, K206Q, R256P and R256W, respectively), (for OAS3 variants: $^{*}p = 0.028$, $p = 0.035$, $p = 0.032$, $p = 0.017$, and $p = 0.034$ for R594C, R767C, R932Q, R932W, and A584T + A722G, respectively; $^{\&}p = 0.059$).

(C) HEK293T-ACE2 cells were transfected with plasmids expressing the *OAS1* WT (as above), *OAS3* WT or the indicated variant genes. At 24 hpt, the cells were mock-infected or infected with SARS-CoV-2, and total RNA was purified 24 h after infection. RNA degradation (bands shown in the red rectangle) was quantified by densitometry and normalized to the amount of the 18S rRNA (shown with an arrow on the left). The levels in mock-treated cells, transfected with the *OAS1*-WT plasmid were expressed as 1, and the other values normalized to this value. Data are represented as mean ± SD. See Figures S3 and S4 for study controls.

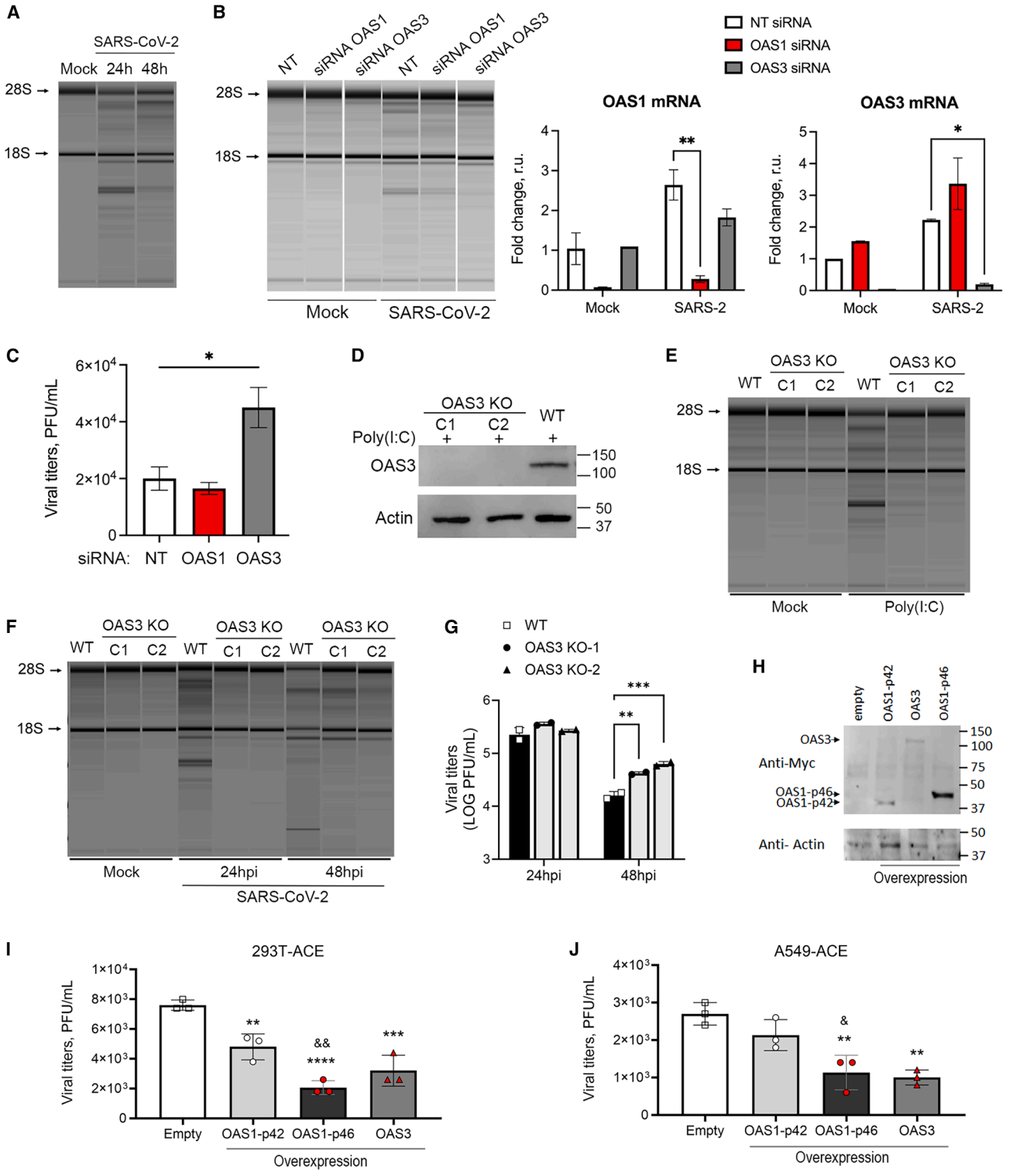

Figure 5. Activation of RNase L after viral infection and effect of OAS3 on RNase L activation

(A) A549-ACE2 cells (rs10774671 A/A genotype) were infected (MOI 1), during 24 and 48 h. Total RNA was purified and analyzed in a Bioanalyzer.

(B) Silencing *OAS1* or *OAS3* with siRNAs reduced the corresponding mRNA expression and attenuated RNA degradation induced by SARS-CoV-2 at 24h. two-way ANOVA and Sidak's multiple comparison test, $^{**}p = 0.002$ for OAS1 mRNA and $^{*}p = 0.010$ for OAS3 mRNA (C) Viral load of silenced cells as assessed by

(legend continued on next page)

of *CCL2* was observed after poly(I:C) or SARS-CoV-2 infection. Among the two samples from patients with ultra-rare LOF variants, sample S2 did not show excessive inflammatory cytokines upon stimulation with poly(I:C) or SARS-CoV-2 (Figures 7B–7D), but it showed high OAS1 expression (Figure S6C). We could argue that high expression of *OAS1* with the rs10774671 G allele in the PBMCs may compensate for the presence of heterozygous rare *OAS3* LOF variants. Conversely, sample S7 showed high cytokine expression. Defective OAS1 binding to dsRNA in the sample carrying the OAS1-K206Q variant could prevent RNase L activation and the degradation of cytokine mRNAs in PBMCs. Since all the ultra-rare variants were found in heterozygosity, the WT allele is expected to partially compensate for the genetic defects.

OAS3-deficient mice show exacerbated inflammatory responses

Given the possibility that defective OAS activity may exaggerate the responses to pro-inflammatory challenges, we investigated the effect of OAS deficiency *in vivo* in mice. We decided to concentrate our study on *Oas3*-deficient mice ($Oas3^{-/-}$), given that in mice *Oas1* possesses 8 paralogs of the human *OAS1* gene. *Oas3* deficiency was validated through genotyping and by examining *Oas3* mRNA expression in the lung following intratracheal administration of poly(I:C) (Figures S7A and S7B). To assess the inflammatory response in the lungs of $Oas3^{-/-}$ and $Oas3^{+/+}$ mice, poly(I:C) was administered daily for 4 days. Treatment did not cause mortality but reduced body weight by up to 15% in both genotypes (Figure S7C). $Oas3^{-/-}$ mice showed higher upregulation of *Ccl2, Cxcl10,* and *Tnf* lung mRNA expression 24h after the last poly (I:C) administration (Figure 8A). Systemically, poly(I:C) treatment increased the concentration of Ccl2 in plasma in both genotypes, with higher increases in $Oas3^{-/-}$ than $Oas3^{+/+}$ mice (Figure 8B). Reduced activation of RNase L in *Oas3*-deficiency could explain the higher expression of pro-inflammatory mRNAs. RNase L degrades ssRNA not only of viral origin but also RNA of the host and, in this way, it limits protein synthesis.[31] We assessed protein synthesis using the surface sensing of translation (SUnSET) method. *Oas3*-deficient mice showed a higher incorporation of puromycin to proteins of the lung than $Oas3^{+/+}$ mice after poly(I:C) treatment (Figure 8C). These results suggest that Oas3 activity results in an attenuation of protein synthesis, which may moderate the expression of pro-inflammatory mediators induced by dsRNA. Histological analysis of the lungs showed preserved parenchymal appearance without cellular infiltrates in the mice of the vehicle group, whereas immune perivascular and peribronchiolar cell infiltrates were detected after poly(I:C) in both genotypes (Figure 8D). Quantification of the density of alveolar epithelium and connective tissue in the histological sections showed a significant increase after poly(I:C), indicative of edema. However, differences between genotypes were not statistically significant (Figure 8D). Mice treated with poly(I:C) developed lymphopenia regardless of their genotype (Figure 8E). In the lung, poly(I:C) increased the percentage of myeloid cells and reduced the proportion of lymphocytes, as assessed by flow cytometry (see gating strategy in Figure S8), but this change was similar in both genotypes (Figures S7D–S7F). Collectively, these results suggest that the enhanced inflammatory response observed in the lungs of $Oas3^{-/-}$ mice challenged with poly(I:C) was not sufficient to cause substantial exacerbation of respiratory pathology, possibly due to the compensatory effects of Oas1 or Oas2 proteins.

Effect of Oas3 on survival, virus replication, and the induction of innate immune responses in mice

We then investigated the response of $Oas3^{-/-}$ and $Oas3^{+/+}$ mice to SARS-CoV-2 infection. Mice were infected with 5,000 PFU of a recombinant SARS-CoV-2 strain adapted to grow in mice (SARS-CoV-2-MA).[52] We performed experiments in male mice since they are more susceptible to SARS-CoV-2 infection.[53] First, we evaluated mortality for 10 days. As expected,[52] we observed mouse death as a consequence of infection. Interestingly, whereas all the $Oas3^{-/-}$ mice succumbed to the infection, 33% of the $Oas3^{+/+}$ mice survived the infection (Figure 9A). Although survival differences among genotypes only exhibited a tendency toward statistical significance, it remains plausible that Oas3 provided a modest level of resistance to SARS-CoV-2-MA infection in mice.

To study whether this effect correlates with virus replication and/or with viral-induced inflammation, another set of mice was infected with SARS-CoV-2-MA, and viral titers and the induction of inflammatory cytokines were studied at different days post-infection (dpi). Viral titers in mouse lungs at day 2 dpi showed no differences between $Oas3^{-/-}$ mice compared to the $Oas3^{+/+}$ mice (Figure 9B). At 4 dpi, lung viral titers showed a non-significant trend toward a slight increase (1.6-fold) in the $Oas3^{-/-}$ mice compared to the $Oas3^{+/+}$ mice (Figure 9B),

measuring the viral titers in the cell culture supernatants using a lysis plaque formation assay. One-way ANOVA and Dunnett's multiple comparisons test (*$p = 0.024$).

(D) Cellular extracts from poly(I:C)-transfected cells were collected and subjected to Western blot analyses using an anti-OAS3 antibody and an anti-actin antibody. Molecular weight markers are indicated (in kDa) on the right.

(E and F) Parental A549-ACE2 and two clones of *OAS3* KO cells were left mock-treated or treated with poly(I:C) (E), or either left mock-infected or infected with SARS-CoV-2 (MOI 1) (F). RNAs were purified and analyzed in a Bioanalyzer 24 hpt (E) or 24 and 48 hpi (F).

(G) Viral titers in the cell culture supernatants of (F) were measured by a lysis plaque formation assay. two-way ANOVA and Tukey's multiple comparison test, **$p = 0.002$, ***$p = 0.0003$.

(H) Cellular extracts from HEK293T-ACE2 mock-infected cells were collected and subjected to Western blot analyses using an anti-myc antibody (to detect OAS1-p42, OAS-p46 and OAS3, indicated by arrows) and an anti-actin antibody. Molecular weight markers are indicated (in kDa) on the right.

(I) HEK293T-ACE2 cells and (J) A549-ACE2 *OAS3* KO cells were transfected with pCAGGS plasmids expressing the *OAS1* WT, *OAS3* WT, or with the empty plasmid, as control. At 24 hpt, the cells were infected with SARS-CoV-2 (MOI 1) for an additional 24 h and viral titers were measured. One-way ANOVA and Sidak's multiple comparison test, symbols indicate comparison vs. 'Empty' (*) or vs. 'OAS1-p42' ($^{\&}$). (I) OAS1-p42 **$p = 0.0065$, OAS1-p46 ****$p < 0.0001$, OAS3 ***$p = 0.0003$; $^{\&\&}p = 0.0076$. (J) OAS1-p46 **$p = 0.0028$, OAS3 **$p = 0.0016$, $^{\&}p = 0.0365$. Data are represented as mean ± SD.

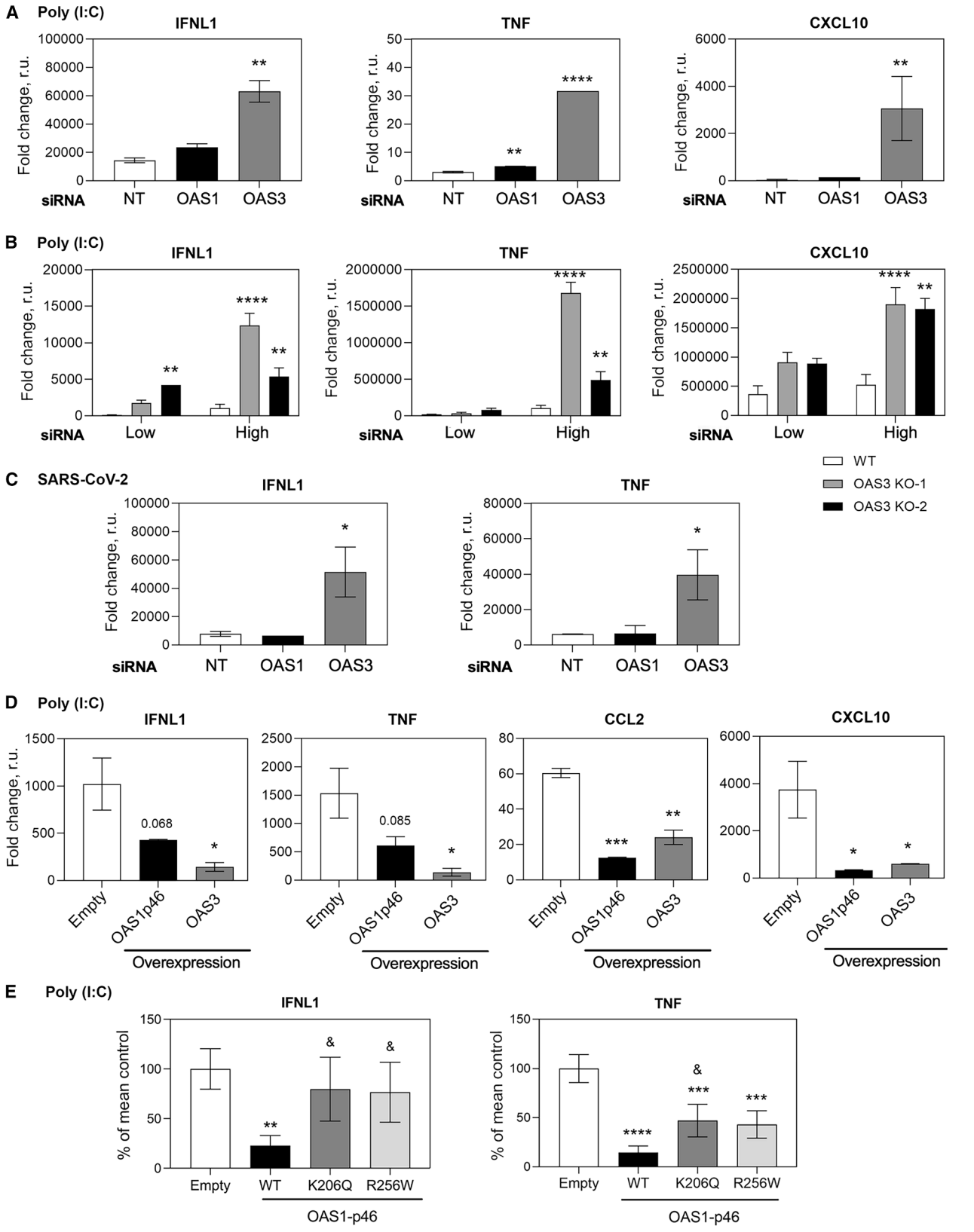

(legend on next page)

suggesting that *Oas3* deficiency does not have a major effect on virus replication in mice. Increased levels of *Oas3* mRNA were observed in infected mice at 2 and 4 dpi, compared to non-infected mice (Figure 9C), showing that *Oas3* expression is highly induced after SARS-CoV-2 infection. Likewise, *Cxcl10* and *Tnf* mRNA in mouse lungs after infection were higher in the $Oas3^{-/-}$ mice as compared to the $Oas3^{+/+}$ mice, and a similar trend was detected for *Ccl2* mRNA, as measured by RT-qPCR 4 dpi (Figure 9D).

SARS-CoV-2 infection also increased the plasma concentration of Cxcl10 and Tnf (Figure 9E), but not Cxcl2 or Ccl5 (not shown), compared to mock-infected mice. Moreover, after the infection, the plasma levels of Cxcl10 were higher in the $Oas3^{-/-}$ than the $Oas3^{+/+}$ mice, and the plasma levels of Tnf-α showed a tendency to increase in the $Oas3^{-/-}$ mice (Figure 9E). Therefore, $Oas3^{-/-}$ mice seem to be prone to develop a more pronounced inflammatory response after the infection. Exacerbated inflammation may contribute to increasing the severity of SARS-CoV-2-induced pathology.[16,17,19]

DISCUSSION

This study identified potentially pathogenic OAS1 and OAS3 missense variants in a population of adult patients (18–65 years old) infected with SARS-CoV-2. It also examined their molecular and functional effects in cells and mice. Since all the variants were found in a heterozygous state, they are unlikely to cause a complete loss of function but could still impair RNase L activity following SARS-CoV-2 infection. Nevertheless, no significant enrichment of these ultra-rare/rare variants was observed in hospitalized or ICU-hospitalized patients compared to non-hospitalized patients. In contrast, for the common OAS1 variant rs10774671 (A/G alleles), we found an increased frequency of the A allele in hospitalized patients within our cohort. Our results showed that OAS1-p42 impaired the antiviral function of the enzymatic system compared to OAS1-p46, consistent with previous studies. However, OAS1-p42 only slightly reduced the enzymatic capacity to generate 2-5A and activate RNase L compared to OAS1-p46, as shown in our enzymatic analysis. Conversely, several ultra-rare/rare variants detected in our cohort of COVID-19 patients were found to be LOF, preventing dsRNA binding and significantly impairing 2-5A production and RNase L activation. Since RNase L degrades ssRNA, including both viral and host cytoplasmic RNA, its activity has a pronounced impact on cellular processes by degrading cytoplasmic mRNA and rRNA, ultimately leading to global protein synthesis inhibition, a common antiviral response. However, ribosomes from translation-arrested cells remain functional, and certain antiviral mRNAs, such as IFN mRNAs, are resistant to RNase L degradation.[31,54] While cells have multiple mechanisms to control viral replication, abolishing RNase L activity is expected to prevent host RNA degradation. This could explain the excessive production of pro-inflammatory cytokine mRNAs and the reduced inhibition of protein synthesis observed in our experimental systems when RNase L activity was impaired. Moreover, RNase L can block nuclear mRNA export and RNA polymerase II-mediated transcription, which limits protein synthesis of type I and III interferon-encoding mRNAs and prevents the expression of interferon stimulated genes (ISGs).[55–57] The loss of negative regulation of cytokine production may contribute to an exaggerated inflammatory response in cells with defective RNase L activation.

By expressing several of the genetic variants found in our cohorts in cellular systems, we found several variants with a deficient capacity to activate RNase L upon infection with SARS-CoV-2 or stimulation with synthetic dsRNA. Moreover, for one of these variants, OAS1-K206Q, we demonstrated the impaired capacity of the recombinant protein to enzymatically produce 2-5A compared to the OAS1-WT protein. 2-5A triggers the activation of RNase L, which then cleaves viral ssRNA and induces IFN-mediated antiviral response.[25] In our study, *OAS3* gene silencing or deficiency impaired the capacity to control viral titers following SARS-CoV-2 infection in cellular systems. Additionally, *OAS3* overexpression slightly lowered viral load, suggesting a modest antiviral role for OAS3 against SARS-CoV-2. However, SARS-CoV-2 infection in *Oas3*-deficient mice did not result in increased viral titers in the lungs, despite these mice showing a tendency toward higher mortality compared to WT mice. Contradictory results are published in the literature regarding the putative anti-viral effect of OAS3. For instance, one study showed

Figure 6. Effect of OAS1 and OAS3 expression on the induction of innate immune responses

(A) A549-ACE2 cells (expressing OAS1-p42) were transfected twice with siRNAs specific for *OAS1* or *OAS3* or with a non-targeted (NT) siRNA. At 24 hpt, the cells were transfected with poly(I:C). Total RNA was purified 24h later for RT-qPCR measurement of the indicated inflammatory mediators. One-way ANOVA and Sidak's multiple comparison test vs. NT, IFNL1: $^{**}p = 0.0038$; TNF: $^{**}p = 0.0025$, $^{***}p < 0.0001$; CXCL10: $^{*}p = 0.0306$).

(B) Parental cells and two clones of OAS3 KO cells were transfected with two different concentrations of poly(I:C) (low: 50 ng/mL and high: 250 ng/mL) or none. At 24h, total RNA was purified for RT-qPCR measurement of the indicated inflammatory mediators. two-way ANOVA and Tukey's multiple comparison test vs. WT, IFNL1: low $^{**}p = 0.0084$, high $^{**}p = 0.0066$, $^{***}+p < 0.0001$; TNF: $^{**}p = 0.0062$, $^{****}p < 0.0001$; CXCL10: $^{**}p = 0.001$; $^{***}p = 0.0007$.

(C) A549-ACE2 cells were transfected twice with siRNAs specific for OAS1 or OAS3 or with a non-targeted (NT) siRNA and were treated with SARS-CoV-2. Inflammatory cytokine mRNA was determined at 24 hpi. One-way ANOVA and Sidak's multiple comparison test vs. NT, IFNL1: $^{*}p = 0.0463$; TNF: $^{*}p = 0.0298$.

(D) OAS3 KO A549-ACE2 cells were transfected with pCAGGS plasmids expressing the OAS1 WT (G/G allele encoding p46) or OAS3 WT forms, or with the empty plasmid, as control. At 24 hpt, the cells were transfected with poly(I:C) and total RNA was purified 24h later. The expression levels of IFNL1, TNF, CCL2, and CXCL10 mRNA were evaluated by RT-qPCR and are expressed as fold change in comparison to cells not exposed to poly(I:C). r.u.: relative units. One-way ANOVA and Sidak's multiple comparison test vs. Empty, IFNL1: $^{*}p = 0.0242$; TNF:$^{*}p = 0.0289$; CCL2: $^{**}p = 0.0019$, $^{***}p = 0.0008$; CXCL10: $^{*}p = 0.0322$ for PAS1p46, $^{*}p = 0.0403$ for OAS3. See also Figure S5.

(E) HEK293T-ACE2 cells were transfected with an empty plasmid, as control, or with plasmids expressing OAS1 rs10774671 (G/G) common genotype either WT or containing rare LOF variant genes. At 24 hpt, the cells were left mock-transfected as controls or transfected with poly(I:C); Total RNA was purified 24 h after poly(I:C) transfection and was analyzed; $n = 4$ samples obtained in two independent experiments. Values were compared vs. control (**) or vs. WT (&) with one-way ANOVA and Sidak's multiple comparison tests. IFNL1: $^{**}p = 0.0026$, $^{\&}p = 0.0215$ $^{\&}p = 0.0215$ for K206Q and $^{\&}p = 0.0296$ for R256W. TNF: $^{****}p < 0.0001$; $^{***}p = 0.0006$ for K206Q, $^{***}p = 0.0003$ for R256W; $^{\&}p = 0.0248$. Data are represented as mean ± SD.

A

Symbol	Variant	Age	Sex	Severity	Genotype rs10774671	sample number
OAS3	V1087M	60	F	Mild	A/G	S1
OAS3	A584T+A722G	37	M	Severe	A/G	S2 (P7)
OAS3	R469=H970=	58	M	Moderate	A/G	S3
OAS3	G1049=	54	F	Severe	A/A	S4
control	none	59	F	Moderate	A/G	S5
OAS3	Y273=	52	F	Moderate	A/G	S6
OAS1	K206Q	61	M	Moderate	A/A	S7 (P4)

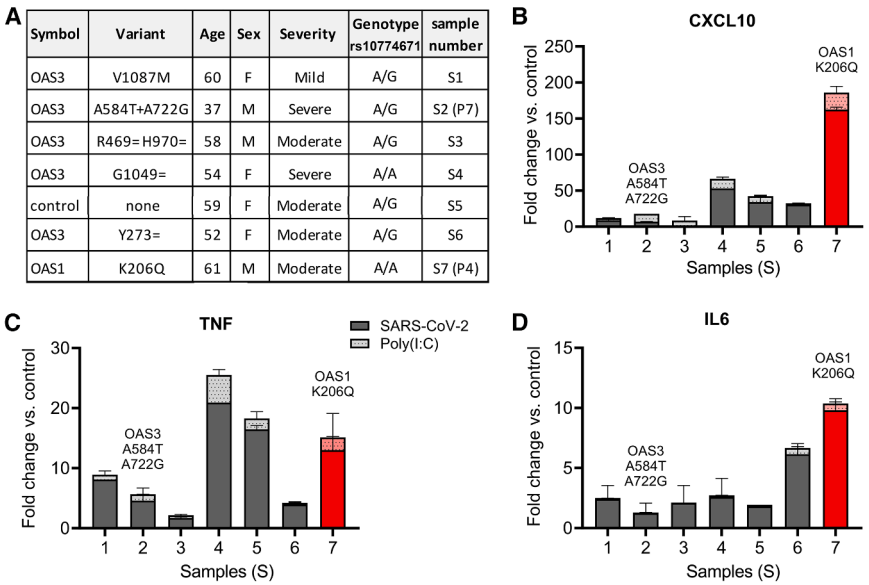

Figure 7. Inflammatory response in PBMCs of patients

(A) Information on the 7 patients from whom we obtained PBMCs and the variants in *OAS1* (red) or *OAS3* carried by them. The column indicating the genotype refers to the *OAS1* rs10774671 common variant. Sample 2 (S2) and S7 corresponded to patients P7 and P4, respectively, as shown in Figure 2. S4 and S7 carried the *OAS1* rs10774671 A/A genotype, whereas the rest of the samples carried the A/G alleles.

(B–D) PBMCs isolated from patient blood were cultured, and 24 h after seeding, the cells were infected with SARS-CoV-2 or treated with poly(I:C) for an additional 24 h (n = 2 replicates per condition). Total RNA was purified and the expression levels of *CXCL10* (B), *TNF* (C) and *IL6* (D) were evaluated by RT-qPCR and expressed as fold change in comparison to non-transfected or non-infected cells. Data are represented as mean ± SD. Also see Figure S6.

that overexpression of OAS3 did not affect SARS-CoV-2 titers,[40] whereas OAS3 was more relevant than OAS1 to induce activation of RNase L and to inhibit virus replication, in human cells infected with Sindbis, Vaccinia, influenza, and West Nile viruses,[46,48] and in bat-derived cells infected with Sindbis and vaccinia viruses.[47] The antiviral activity of OAS3 arises from its high capacity to condense viral dsRNA and activate RNase L.[48] However, a recent study showed that RNase L deficient cells only showed a mild increase in the susceptibility to SARS-CoV-2 infection relative to WT cells, and *OAS1* KO cells did not show a higher proportion of infection after exposure to SARS-CoV-2.[43]

The effects of OAS1 are complex due to the presence of several common variants widely distributed in the population. Among these, the *OAS1* rs10774671 SNP has garnered particular attention, as previous studies in hospitalized SARS-CoV-2 patients revealed that the G allele was associated with a slight protective effect against severe COVID-19 (37). The G allele encodes an OAS1 isoform (p46) that undergoes prenylation, enabling greater antiviral activity against SARS-CoV-2, whereas the shorter isoform (p42), encoded by the A allele, lacks this capability (37). Accordingly, it has been reported that overexpression of OAS1 p46 isoform in cells decreased viral titers, whereas overexpression of OAS1 p42 isoform did not.[40] However, a previous study showed that overexpression of several OAS1 isoforms in HEK293T cells did not alter the capacity to activate RNase L in response to poly(I:C), although these experiments were performed by overexpressing the different isoforms, not under physiological conditions.[58] In line with this report, we found that the p42 and p46 OAS1 isoforms had similar effects on rRNA degradation following poly(I:C) exposure after protein overexpression. Despite the capacity to activate RNase L, we found that p46 was more effective than p42 in restricting viral load after SARS-CoV-2 infection following overexpression of p42 or p46, including cells lacking OAS3. Additionally, *OAS1* gene silencing in cells naturally expressing OAS1-p42 had no effect on viral titers. Altogether, these findings suggest that OAS1-p42 can activate RNase L in the cytoplasm, but it is defective in viral restriction, likely because it cannot detect viral particles accumulated in intracellular organelles, as, unlike OAS1-p46, it is unable to undergo prenylation and localization in cellular membranes.[37,45,50] To explore the expected differential effects of p42 and p46 OAS1 isoforms on viral restriction in COVID-19, we analyzed their association with clinical outcomes in a Spanish cohort of patients infected with SARS-CoV-2. The p42 isoform was notably enriched in hospitalized patients compared to non-hospitalized ones, with an even stronger enrichment in ICU patients compared to non-hospitalized individuals, in agreement with the previous GWAS studies. Conversely, we did not identify a significant correlation between heterozygous OAS1 and OAS3 LOF variants and severe hypoxemia in adult COVID-19 patients. Consistently, with our findings, adult family members of the previously reported MIS-C children with recessive deficiencies of the OAS-RNase L pathway, who were heterozygous for the same deleterious variant as that of the MIS-C patients, did not report any hospitalization due to severe COVID-19.[43]

Compensatory functional effects among the various OAS proteins may explain the lack of clinical enrichment for rare LOF variants. It is also important to note that all OAS1 and OAS3 variants identified were in the heterozygous state, making complete LOF unlikely. Moreover, while OAS1 variants exhibit LOF in terms of RNase L activation, we cannot rule out the possibility that they retain recently described non-canonical functions.[50,59] Specifically, OAS1-p46 binds to AU-rich elements (AREs) in certain mRNAs, most notably IFNB mRNA, protecting them from degradation by the mRNA decay machinery and thereby increasing their stability.[50] This mechanism may contribute to the antiviral activity of OAS1-p46. In addition, OAS1-p46 has been shown to bind IRF1 mRNA, enhancing its translation and further boosting host immune responses.[59] Furthermore, OAS1-p46 may function in an RNase L-independent manner to interfere with viral RNA functions, as it induces aggregation of West Nile virus

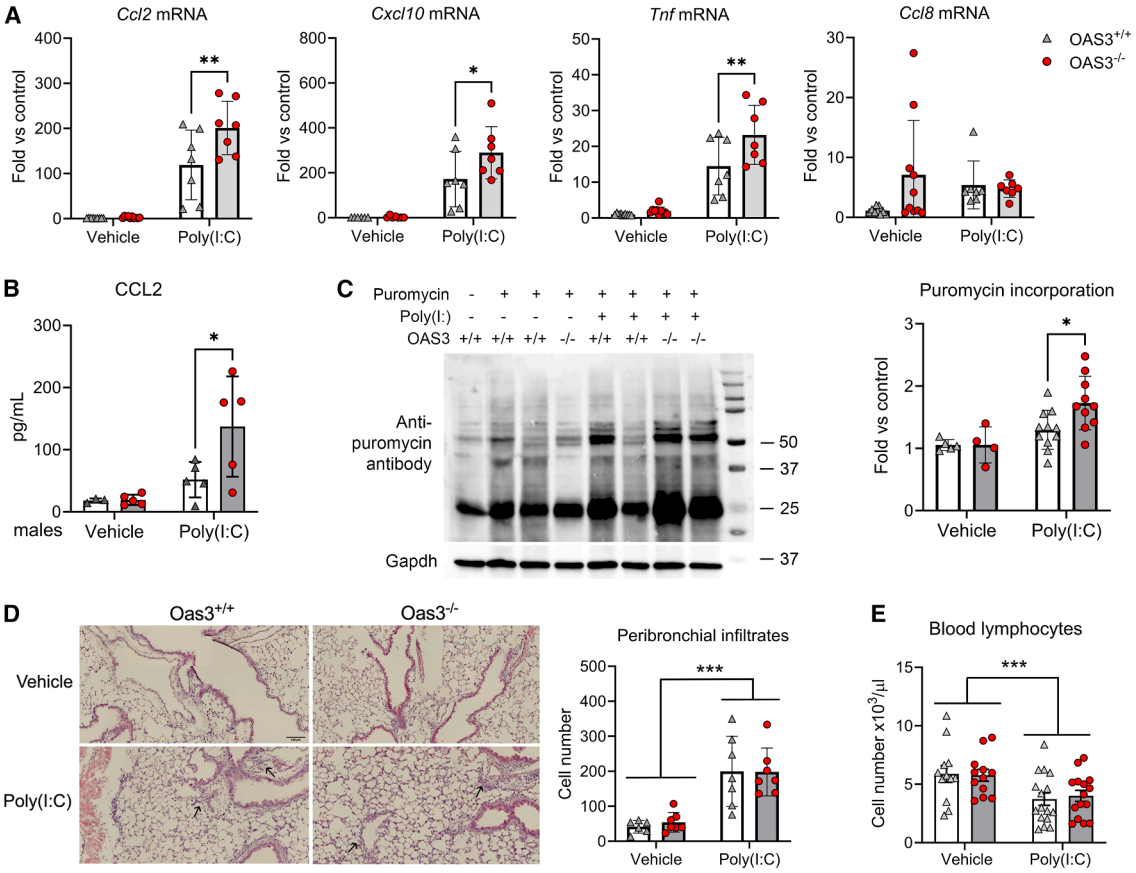

Figure 8. Oas3-deficient mice show a higher inflammatory response in the lungs

Oas3$^{-/-}$ and *Oas3*$^{+/+}$ mice (n = 7 per group), male and females, received 4 daily intratracheal administrations of 60 µL poly(I:C) (1 µg/mL sterile H_2O) or vehicle for 4 days. One day after the last administration, lungs and blood were collected.

(A) Lungs were collected for mRNA studies by RT-qPCR. After poly(I:C) treatment, *Oas3*$^{-/-}$ mice showed higher mRNA expression of *Ccl2* (**p = 0.003), *Cxcl10* (*p = 0.037) and *Tnf* (**p = 0.009) (two-way ANOVA by genotype and treatment), but not *Ccl8* mRNA. Values are expressed as fold versus control (mean of vehicle in *Oas3*$^{+/+}$ group). Bars show the mean ± SD and points correspond to individual mice.

(B) Plasma Ccl2 concentration (n = 7–10 per group) increased after poly(I:C) in both genotypes. There was a trend toward a higher increase in *Oas3*$^{-/-}$ group (p = 0.097, Mann-Whitney test).

(C) Protein synthesis was assessed with the SUnSET method. *p = 0.014, two-way ANOVA and Šídák's multiple comparisons test; for each genotype, n = 3–6 mice in the vehicle groups and n = 10–11 mice in the poly(I:C) groups. Gapdh is the loading control. Std: standard for molecular mass; values (kDa) shown on the right.

(D) Representative histological sections of lungs stained with hematoxylin and eosin. Arrows indicate peribronchial infiltrates (two-way ANOVA, n = 7 per group, ***p < 0.0001 poly(I:C) vs. vehicle, for each genotype). Scale bar: 100 µm.

(E) Blood lymphocytes were measured in a hemocytometer. Effect of poly(I:C) (***p < 0.0001, two-way ANOVA) (n = 12–16 per group). Data are represented as mean ± SD. See Figures S7 and S8.

ssRNA genomes but does not initiate RNase L-mediated mRNA decay.[48] If such non-canonical activities were retained in the described rare LOF variants on the rs10774671 G genotype, they may still confer partial antiviral protection, potentially mitigating the impact of RNase L LOF on susceptibility to severe COVID-19. We believe that the non-canonical functions of OAS proteins warrant further investigation, as they may offer new insights into antiviral defense mechanisms beyond RNase L activation.

Some COVID-19 patients develop a cytokine storm characterized by excessive production of chemokines and other cytokines.[60,61] Previous studies in human macrophages showed that OAS1 and OAS3 negatively regulate the expression of chemokines and IFN-responsive genes.[43,62] Our findings suggest that defects in OAS1 and OAS3 are associated with an amplified inflammatory response in human A549-ACE2 cells following exposure to SARS-CoV-2 or dsRNA, and that the anti-inflammatory effect of OAS1-p46 may be attenuated in OAS1-p42, as silencing OAS1 in cells naturally expressing p42 results in only a small increase in the cytokine response. Moreover, the capacity of OAS1-p46 to control inflammatory cytokine mRNA expression was lost when the OAS1 gene carried LOF rare variants. In mice, we observed a slightly heightened inflammatory response in *Oas3* KO mice compared to corresponding WT mice following

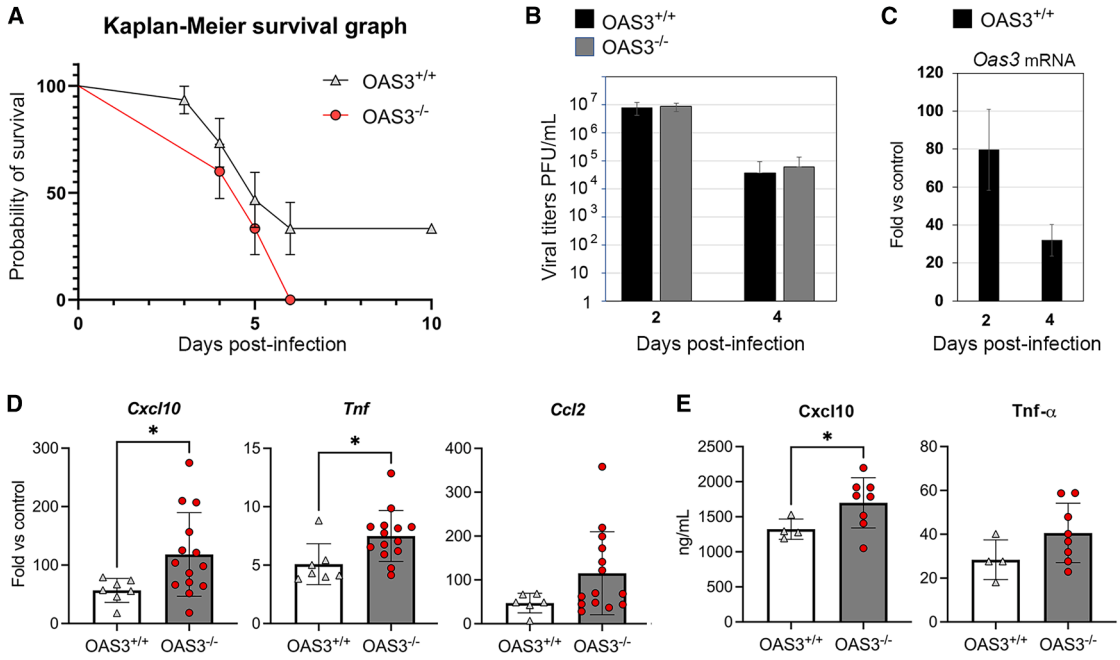

Figure 9. Oas3 expression slightly counteracts the induction of inflammatory responses *in vivo*

(A) *Oas3*$^{-/-}$ (KO) and *Oas3*$^{+/+}$ (WT) male mice (n = 15/group) were infected with a mouse-adapted SARS-CoV-2-MA virus (5,000 PFU/mice), and mice survival was evaluated daily. Mice losing more than 25% of their initial weight were humanely euthanized and considered as part of viral-induced mortality. Survival curves (Chi Square, p = 0.09).

(B–E) *Oas3*$^{+/+}$ and *Oas3*$^{-/-}$ mice (n = 4 for both *Oas3*$^{+/+}$ and *Oas3*$^{-/-}$ mice 2 dpi, and n = 7 and 14 for *Oas3*$^{+/+}$ and *Oas3*$^{-/-}$ mice, respectively, at 4 dpi) were infected with a SARS-CoV-2-MA virus (5,000 PFU/mice).

(B) Viral titers in mouse lungs were evaluated 2 and 4 dpi.

(C) The expression of *Oas3* mRNA in *Oas3*$^{+/+}$ mice was evaluated by RT-qPCR at 2 and 4 dpi.

(D) The expression of *Cxcl10*, *Tnf* and *Ccl2* mRNA was evaluated in mouse lungs by RT-qPCR 4 dpi. mRNA levels were expressed as fold change (increases) in comparison to mock-infected mice, used as controls. *Cxcl10* (*p = 0.040, t test), *Tnf* (*p = 0.016, Mann-Whitney test) and *Ccl2* (p = 0.179, Mann-Whitney test).

(E) The expression of *Cxcl10* and Tnf proteins was evaluated in mouse sera (n = 4 and 8 for *Oas3*$^{+/+}$ and *Oas3*$^{-/-}$ mice, respectively) at 4 dpi. *Cxcl10* (*p = 0.038, t test) and Tnf (p = 0.069, t test). Data are represented as mean ± SD.

poly(I:C) treatment or SARS-CoV-2 infection. Impaired OAS activity reduces RNase L functionality. RNase L can degrade not only viral ssRNA but also host mRNA, thereby exerting an inhibitory effect on protein synthesis.[31] It is conceivable that degradation of host mRNA is reduced in *Oas3*-deficient mice after infection, thereby facilitating the expression of pro-inflammatory molecules. Supporting this notion, we observed that the higher inflammatory responses in *Oas3*-deficient mice were accompanied by elevated protein synthesis. Consequently, a deficient OAS system may result in the loss of a fundamental regulatory mechanism for controlling the induction of inflammatory mediators. While these effects may amplify the host's inflammatory reactions, they seem to be partially independent of the antiviral response.

While our experimental results highlight a role of OAS1 and OAS3 as negative regulators of inflammatory responses triggered by dsRNA and SARS-CoV-2 infection in cells and mice, we could only demonstrate an association of the (A/A) genotype of the common rs10774671 OAS1 variant with the pathophysiology of COVID-19 pneumonia in adults. Following SARS-CoV-2 infection in children, autosomal recessive deficiencies in the OAS-RNase L system increase inflammation, facilitating SARS-CoV-2–related MIS-C unrelated to hypoxemic pneumonia.[43] The molecular mechanism underlying this delayed hyperinflammatory response detected in children with a deficient OAS-RNase L system is intriguing. Deficient production of 2-5A, insufficient activation of RNase L, and reduced inhibitory control on the mitochondrial antiviral-signaling protein (MAVS) pathway in macrophages are likely involved.[43] The reason why hyperinflammation manifests in a delayed fashion following viral exposure in children is unknown, but it may suggest the need for some process of training of the innate immune system. Whether this effect is unique to the immature immune system of children or may also manifest in adult patients with a deficient OAS-RNase L pathway, where the effects could present as delayed complications unrelated to respiratory pathology, remains uncertain.

In summary, our study underscores the role of OAS1 and OAS3 in limiting inflammatory responses triggered by SARS-CoV-2 infection or dsRNA treatment in both human cells and mice. Additionally, our findings suggest that while OAS1-p46 and OAS3 exhibit some antiviral activity, OAS1-p42 is ineffective at controlling viral load in cellular systems. Supporting this observation, the A/A genotype of the OAS1 rs10774671 SNP was associated with increased disease severity in our cohort

of COVID-19 patients. However, the presence of rare heterozygous *OAS1* or *OAS3* LOF variants in adult COVID-19 patients was not linked to more severe respiratory outcomes. Further research is needed to determine whether these variants, particularly in monoallelic or biallelic states, might predispose individuals to delayed systemic inflammatory complications of COVID-19.

Limitations of the study

Limitations of our study include the possibility that some patients may have undetermined factors influencing disease severity, such as type I IFN autoantibodies, alterations in inflammatory pathways, differences in inoculum dosage, or co-morbidities like obesity, that could have obscured clear enrichment signals in our analysis. For example, obese individuals without the genetic variants under study might still develop severe COVID-19, as elevated BMI is an established risk factor for worse outcomes. Finally, not including infections with the mouse-adapted SARS-CoV-2 strain in female mice is another limitation of the study. However, we chose to focus on male mice because of the worse outcomes observed in men infected with SARS-CoV-2, consistent with previous reports in both humans[44,45] and mice,[53,63] and with a significantly increased proportion of men in the most severely affected individuals observed in the Spanish cohort.

RESOURCE AVAILABILITY

Lead contact

Anna M. Planas, PhD.

Department of Neuroscience and Experimental Therapeutics, Institute for Biomedical Research of Barcelona (IIBB), Spanish National Research Council (CSIC) Rosselló-161, planta 6, E−08036-Barcelona, Spain e-mail: anna.planas@iibb.csic.es.

Materials availability

Main data are available in the main text and supplementary material. Other materials and procedures will be made available upon reasonable request.

Data and code availability

- Data: Genetic sequencing data have been deposited on the European Genome-phenome Archive (EGA: EGAD50000000094).
- Code: All scripts created for the bioinformatic analysis of the genetic results can be found at https://doi.org/10.5281/zenodo.17396248.
- Other data will be made available upon reasonable request.

CONSORTIA

Covid Human Genetic Effort: Laurent Abel, Alessandro Aiuti, Evangelos Andreakos, Andrés A. Arias, Hagit Baris Feldman, Alexandre Belot, Catherine M. Biggs, Anastasiia Bondarenko, Alessandro Borghesi, Ahmed A. Bousfiha, Petter Brodin, Manish J. Butte, Giorgio Casari, John Christodoulou, Antonio Condino-Neto, Clifton L. Dalgard, Munïs Dundar, Sara Espinosa-Padilla, Jacques Fellay, Carlos Flores, José Luis Franco, Guy Gorochov, Peter K. Gregersen, Rabih Halwani, Lennart Hammarström, Elena W.Y. Hsieh, Yuval Itan, Tom Le Voyer, Yu-Lung Lau, Davood Mansouri, Isabelle Meyts, Trine H. Mogensen, Lisa F.P. Ng, Antonio Novelli, Giuseppe Novelli, Satoshi Okada, Keisuke Okamoto, Qiang Pan-Hammarström, Rebeca Perez de Diego, Graziano Pesole, Anna M. Planas, Aurora Pujol, Lluis Quintana-Murci, Laurent Renia, Igor Resnick, Carlos Rodríguez-Gallego, Lee Rowen, Mohammed Shahrooei, Pere Soler-Palacín, Ivan Tancevski, Stuart G. Tangye, Ahmad Abou Tayoun, Sehime G. Temel, Christian Thorball, Stuart E. Turvey, K. M. Furkan Uddin, Mohammed J. Uddin, Diederik van de Beek, Donald C. Vinh, Mayana Zatz, Qian Zhang, Helen C. Su, and Jean-Laurent Casanova. The corresponding affiliations are provided in a supplemental information.

ACKNOWLEDGMENTS

Supported by the Spanish National Research Council (CSIC) through the Fondo COVID-19 (Ref. CSIC-202020E086). This research work was also funded by the European Commission – NextGenerationEU (Regulation EU 2020/2094), through CSIC's Global Health Platform (PTI Salud Global). Funds were also provided by the Spanish Ministry of Science and Innovation, PID2021-123810OB-I00 funded by MCIN/AEI/10.13039/50110.00110.33 and CNS2022-135276. We acknowledge the EASI-Genomics initiative (PID12396) that received funds from the European Union's Horizon 2020 research and innovation program under grant agreement No. 824110.

We are indebted to the nursing staff at Hospital Clínic and to the patients for their generous donation, to Fundació Glòria Soler for its support to the COVIDBANK initiative, and to the HCB-IDIBAPS Biobank for the biological human samples and data procurement. We acknowledge the collaboration of IBSP-CV (PT17/0015/0017), ISABIAL, INCLIVA (PT17/0015/0049, B:000768 ISCIII), and La Fe biobanks, integrated in the Spanish National Biobanks Network and the Valencian Biobanking Network. We thank Prof. Luis Enjuanes (Centro Nacional de Biotecnología-CSIC, Spain) for providing us with the mouse-adapted SARS-CoV-2 strain. We thank Dr. Victor Peinado and Dr. Anna Serrano (IIBB-CSIC) for their advice on the assessment of lung pathological features in mice. Protein production and purification have been performed by the ICTS "NANBIOSIS", specifically by the Protein Production Platform of CIBER in Bioengineering, Biomaterials & Nanomedicne (CIBER-BBN, ISCIII)/IBB, at the Universitat Autònoma de Barcelona (http://www.nanbiosis.es/portfolio/u1-protein-production-platform-ppp/). ChimeraX was developed by the Resource for Biocomputing, Visualization, and Informatics at the University of California, San Francisco, with support from the National Institutes of Health R01-GM129325 and the Office of Cyber Infrastructure and Computational Biology and intramural Research Program of the National Institute of Allergy and Infectious Diseases. The Laboratory of Human Genetics of Infectious Diseases is supported by the Howard Hughes Medical Institute, the Rockefeller University, the St. Giles Foundation, the National Institutes of Health (NIH) (R21AI160576), the National Center for Advancing Translational Sciences (NCATS), NIH Clinical and Translational Science Award (CTSA) program (UL1TR001866), the Fisher Center for Alzheimer's Research Foundation, the Meyer Foundation, the JPB Foundation, the French National Research Agency (ANR) under the "Investments for the Future" program (ANR-10-IAHU-01), the Integrative Biology of Emerging Infectious Diseases Laboratory of Excellence (ANR-10-LABX-62-IBEID), the French Foundation for Medical Research (FRM) (EQU201903007798), the ANR GenMISC (ANR-21-COVR-039), the European Union's Horizon 2020 research and innovation program under grant agreement No. 824110 (EASI-genomics), the HORIZON-HLTH-2021-DISEASE-04 program under grant agreement 101057100 (UNDINE), the ANR-RHU Program ANR-21-RHUS-08 (COVIFERON), the Square Foundation, Grandir - Fonds de solidarité pour l'enfance, the Fondation du Souffle, the SCOR Corporate Foundation for Science, the Battersea & Bowery Advisory Group, William E. Ford, General Atlantic's Chairman and Chief Executive Officer, Gabriel Caillaux, General Atlantic's Co-President, Managing Director and Head of business in EMEA, and the General Atlantic Foundation, the French Ministry of Higher Education, Research, and Innovation (MESRI-COVID-19), Institut National de la Santé et de la Recherche Médicale (INSERM), Imagine Institute, and Paris Cité University. D.L was supported by the European Society for Immunodeficiencies bridge grant and a fellowship from the FRM. H.C.S. was supported by the Intramural Research Program of the NIAID, NIH.

AUTHOR CONTRIBUTIONS

Provision of samples and/or clinical data: Oriol Sibila, Rosa Faner, Pedro Castro, Carlos Domingo, Verónica Robles, Josep L. Bedini, Veronica Rico, Daiana Aguero, Alex Soriano, Francisco Lozano, Andrea Martín Nalda, Alba Parra Martínez, Roger Colobrán, Pere Soler-Palacín, Alexandre Serra-Llovich, Beatriz Dietl, M[a] Jesús Arranz, David Dalmau, Jaime Signes-Costa, Joan Gil-Carbonell, José Todoli, Jacobo Martínez, Silvia Rojo, Aida Fiz-López, Elisa Arribas, Paloma Cal-Sabater, David Bernado, Shen-Ying Zhang, Helen Su, Hassan Abolhassani, Qiang Pan Hammarström, and Aurora Pujol.

Investigation and methodology: Raúl López-Fernández-Sobrino, Darío López-García, Laia Llucià-Carol, Jordi Pedragosa, Vanessa Rivero, Paula Vázquez, Laura Palomo Sánchez-Grande, Francisca Ruiz-Jaén, Leonardo Márquez-Kisinousky, Aitor Nogales, Marta L DeDiego, and Jordi Pérez-Tur.

Genetic data: Jordi-Pérez-Tur, Jordi Durban, Fernando Cardona, Marina Vogel, and Stefan Wiemann.

Data analysis: Jordi Durbán, Jordi Pérez-Tur, Miriam Cobo, Lara Lloret, Jordi Pedragosa, Marta L. DeDiego, and Anna M. Planas.

Review and editing: Helen Su, Danyel Lee, Shen-Ying Zhang, Jean-Laurent Casanova, Pere Soler, Aitor Nogales, Hassan Abolhassani, and Pedro Castro.

Conceptualization, data curation, formal analysis, funding acquisition, resources, supervision, validation, visualization, writing – original draft, and writing – review & editing: Marta L DeDiego (corresponding author for cellular studies and infection experiments), Israel Fernández-Cadenas, Jordi Pérez-Tur (corresponding author for human genetic studies), and Anna M. Planas (corresponding author for the global study and lead contact).

DECLARATION OF INTERESTS

The authors declare no competing interests.

STAR★METHODS

Detailed methods are provided in the online version of this paper and include the following:

- KEY RESOURCES TABLE
- EXPERIMENTAL MODEL AND STUDY PARTICIPANT DETAILS
  - Human subjects and ethics
  - Animal studies and ethics
- METHOD DETAILS
  - Whole exome sequencing
  - Structural modeling
  - Alignment
  - Selection of variants to analyze their functional effect
  - Determining the phase of multiple *OAS* variants in the same individual
  - Cell lines
  - Viruses and virus titrations
  - Plasmids
  - Generation of A549 *OAS3* KO cells
  - Overexpression of hACE-2 in A549 and HEK293T cells
  - Effect of OAS1 and OAS3 variants on RNA integrity
  - Effect of OAS1 and OAS3 variants on protein expression
  - siRNA-mediated silencing
  - Western blot
  - Effect of OAS1 and OAS3 variants on innate immune responses
  - RT-qPCR
  - Isolation of peripheral blood mononuclear cells (PBMCs)
  - Generation of human recombinant wild type and mutant OAS1 proteins
  - OAS1 enzymatic activity
  - Intratracheal administration of poly(I:C) and sample processing
  - Mouse infection with a mouse-adapted SARS-CoV-2 viral strain
- QUANTIFICATION AND STATISTICAL ANALYSIS
  - Power analysis for the human studies
  - Regression analysis
  - Analysis pipeline
  - Gene-based association analysis
  - Analysis of rs10774671
  - Statistical methods for animal studies

SUPPLEMENTAL INFORMATION

Supplemental information can be found online at https://doi.org/10.1016/j.isci.2025.113966.

Received: July 22, 2024
Revised: August 15, 2025
Accepted: November 4, 2025
Published: November 11, 2025

REFERENCES

1. Zhang, Q., Bastard, P., Liu, Z., Le Pen, J., Moncada-Velez, M., Chen, J., Ogishi, M., Sabli, I.K.D., Hodeib, S., Korol, C., et al. (2020). Inborn errors of type I IFN immunity in patients with life-threatening COVID-19. Science *370*, eabd4570. https://doi.org/10.1126/science.abd4570.
2. Zhang, Q., Bastard, P., Bolze, A., Jouanguy, E., Zhang, S.-Y., COVID Human Genetic Effort, Cobat, A., Notarangelo, L.D., Su, H.C., Abel, L., and Casanova, J.L. (2020). Life-Threatening COVID-19: Defective Interferons Unleash Excessive Inflammation. Med *1*, 14–20. https://doi.org/10.1016/j.medj.2020.12.001.
3. Asano, T., Boisson, B., Onodi, F., Matuozzo, D., Moncada-Velez, M., Maglorius Renkilaraj, M.R.L., Zhang, P., Meertens, L., Bolze, A., Materna, M., et al. (2021). X-linked recessive TLR7 deficiency in ~1% of men under 60 years old with life-threatening COVID-19. Sci. Immunol. *6*, eabl4348. https://doi.org/10.1126/sciimmunol.abl4348.
4. Onodi, F., Bonnet-Madin, L., Meertens, L., Karpf, L., Poirot, J., Zhang, S.-Y., Picard, C., Puel, A., Jouanguy, E., Zhang, Q., et al. (2021). SARS-CoV-2 induces human plasmacytoid predendritic cell diversification via UNC93B and IRAK4. J. Exp. Med. *218*, e20201387. https://doi.org/10.1084/jem.20201387.
5. van der Made, C.I., Simons, A., Schuurs-Hoeijmakers, J., van den Heuvel, G., Mantere, T., Kersten, S., van Deuren, R.C., Steehouwer, M., van Reijmersdal, S.V., Jaeger, M., et al. (2020). Presence of Genetic Variants Among Young Men With Severe COVID-19. JAMA *324*, 663–673. https://doi.org/10.1001/jama.2020.13719.
6. Fallerini, C., Daga, S., Mantovani, S., Benetti, E., Picchiotti, N., Francisci, D., Paciosi, F., Schiaroli, E., Baldassarri, M., Fava, F., et al. (2021). Association of Toll-like receptor 7 variants with life-threatening COVID-19 disease in males: findings from a nested case-control study. eLife *10*, e67569. https://doi.org/10.7554/eLife.67569.
7. Mantovani, S., Daga, S., Fallerini, C., Baldassarri, M., Benetti, E., Picchiotti, N., Fava, F., Gallì, A., Zibellini, S., Bruttini, M., et al. (2022). Rare variants in Toll-like receptor 7 results in functional impairment and downregulation of cytokine-mediated signaling in COVID-19 patients. Genes Immun. *23*, 51–56. https://doi.org/10.1038/s41435-021-00157-1.
8. Zhang, Q., Matuozzo, D., Le Pen, J., Lee, D., Moens, L., Asano, T., Bohlen, J., Liu, Z., Moncada-Velez, M., Kendir-Demirkol, Y., et al. (2022). Recessive inborn errors of type I IFN immunity in children with COVID-19 pneumonia. J. Exp. Med. *219*, e20220131. https://doi.org/10.1084/jem.20220131.
9. Bastard, P., Rosen, L.B., Zhang, Q., Michailidis, E., Hoffmann, H.-H., Zhang, Y., Dorgham, K., Philippot, Q., Rosain, J., Béziat, V., et al. (2020). Autoantibodies against type I IFNs in patients with life-threatening COVID-19. Science *370*, eabd4585. https://doi.org/10.1126/science.abd4585.
10. Bastard, P., Gervais, A., Le Voyer, T., Rosain, J., Philippot, Q., Manry, J., Michailidis, E., Hoffmann, H.-H., Eto, S., Garcia-Prat, M., et al. (2021). Autoantibodies neutralizing type I IFNs are present in ~4% of uninfected

individuals over 70 years old and account for ~20% of COVID-19 deaths. Sci. Immunol. *6*, eabl4340. https://doi.org/10.1126/sciimmunol.abl4340.

11. Bastard, P., Gervais, A., Taniguchi, M., Saare, L., Särekannu, K., Le Voyer, T., Philippot, Q., Rosain, J., Bizien, L., Asano, T., et al. (2024). Higher COVID-19 pneumonia risk associated with anti-IFN-α than with anti-IFN-ω auto-Abs in children. J. Exp. Med. *221*, e20231353. https://doi.org/10.1084/jem.20231353.
12. Shaw, A.E., Hughes, J., Gu, Q., Behdenna, A., Singer, J.B., Dennis, T., Orton, R.J., Varela, M., Gifford, R.J., Wilson, S.J., and Palmarini, M. (2017). Fundamental properties of the mammalian innate immune system revealed by multispecies comparison of type I interferon responses. PLoS Biol. *15*, e2004086. https://doi.org/10.1371/journal.pbio.2004086.
13. Channappanavar, R., Fehr, A.R., Vijay, R., Mack, M., Zhao, J., Meyerholz, D.K., and Perlman, S. (2016). Dysregulated Type I Interferon and Inflammatory Monocyte-Macrophage Responses Cause Lethal Pneumonia in SARS-CoV-Infected Mice. Cell Host Microbe *19*, 181–193. https://doi.org/10.1016/j.chom.2016.01.007.
14. Crow, M.K., Olferiev, M., and Kirou, K.A. (2019). Type I Interferons in Autoimmune Disease. Annu. Rev. Pathol. *14*, 369–393. https://doi.org/10.1146/annurev-pathol-020117-043952.
15. Lee, J.S., and Shin, E.-C. (2020). The type I interferon response in COVID-19: implications for treatment. Nat. Rev. Immunol. *20*, 585–586. https://doi.org/10.1038/s41577-020-00429-3.
16. Costela-Ruiz, V.J., Illescas-Montes, R., Puerta-Puerta, J.M., Ruiz, C., and Melguizo-Rodríguez, L. (2020). SARS-CoV-2 infection: The role of cytokines in COVID-19 disease. Cytokine Growth Factor Rev. *54*, 62–75. https://doi.org/10.1016/j.cytogfr.2020.06.001.
17. Tang, Y., Liu, J., Zhang, D., Xu, Z., Ji, J., and Wen, C. (2020). Cytokine Storm in COVID-19: The Current Evidence and Treatment Strategies. Front. Immunol. *11*, 1708. https://doi.org/10.3389/fimmu.2020.01708.
18. Ruan, Q., Yang, K., Wang, W., Jiang, L., and Song, J. (2020). Clinical predictors of mortality due to COVID-19 based on an analysis of data of 150 patients from Wuhan, China. Intensive Care Med. *46*, 846–848. https://doi.org/10.1007/s00134-020-05991-x.
19. Yang, L., Xie, X., Tu, Z., Fu, J., Xu, D., and Zhou, Y. (2021). The signal pathways and treatment of cytokine storm in COVID-19. Signal Transduct. Target. Ther. *6*, 255. https://doi.org/10.1038/s41392-021-00679-0.
20. Sola, I., Almazán, F., Zúñiga, S., and Enjuanes, L. (2015). Continuous and Discontinuous RNA Synthesis in Coronaviruses. Annu. Rev. Virol. *2*, 265–288. https://doi.org/10.1146/annurev-virology-100114-055218.
21. Goubau, D., Deddouche, S., and Reis e Sousa, C. (2013). Cytosolic sensing of viruses. Immunity *38*, 855–869. https://doi.org/10.1016/j.immuni.2013.05.007.
22. Lamborn, I.T., and Su, H.C. (2020). Genetic determinants of host immunity against human rhinovirus infections. Hum. Genet. *139*, 949–959. https://doi.org/10.1007/s00439-020-02137-3.
23. Hornung, V., Hartmann, R., Ablasser, A., and Hopfner, K.-P. (2014). OAS proteins and cGAS: unifying concepts in sensing and responding to cytosolic nucleic acids. Nat. Rev. Immunol. *14*, 521–528. https://doi.org/10.1038/nri3719.
24. Dong, B., and Silverman, R.H. (1995). 2-5A-dependent RNase molecules dimerize during activation by 2-5A. J. Biol. Chem. *270*, 4133–4137. https://doi.org/10.1074/jbc.270.8.4133.
25. Sadler, A.J., and Williams, B.R.G. (2008). Interferon-inducible antiviral effectors. Nat. Rev. Immunol. *8*, 559–568. https://doi.org/10.1038/nri2314.
26. Schwartz, S.L., and Conn, G.L. (2019). RNA regulation of the antiviral protein 2'-5'-oligoadenylate synthetase. Wiley Interdiscip. Rev. RNA *10*, e1534. https://doi.org/10.1002/wrna.1534.
27. Malathi, K., Dong, B., Gale, M., and Silverman, R.H. (2007). Small self-RNA generated by RNase L amplifies antiviral innate immunity. Nature *448*, 816–819. https://doi.org/10.1038/nature06042.
28. Iordanov, M.S., Paranjape, J.M., Zhou, A., Wong, J., Williams, B.R., Meurs, E.F., Silverman, R.H., and Magun, B.E. (2000). Activation of p38 mitogen-activated protein kinase and c-Jun NH(2)-terminal kinase by double-stranded RNA and encephalomyocarditis virus: involvement of RNase L, protein kinase R, and alternative pathways. Mol. Cell Biol. *20*, 617–627. https://doi.org/10.1128/MCB.20.2.617-627.2000.
29. Rath, S., Donovan, J., Whitney, G., Chitrakar, A., Wang, W., and Korennykh, A. (2015). Human RNase L tunes gene expression by selectively destabilizing the microRNA-regulated transcriptome. Proc. Natl. Acad. Sci. USA *112*, 15916–15921. https://doi.org/10.1073/pnas.1513034112.
30. Donovan, J., Rath, S., Kolet-Mandrikov, D., and Korennykh, A. (2017). Rapid RNase L-driven arrest of protein synthesis in the dsRNA response without degradation of translation machinery. RNA *23*, 1660–1671. https://doi.org/10.1261/rna.062000.117.
31. Burke, J.M., Moon, S.L., Matheny, T., and Parker, R. (2019). RNase L Reprograms Translation by Widespread mRNA Turnover Escaped by Antiviral mRNAs. Mol. Cell *75*, 1203–1217.e5. https://doi.org/10.1016/j.molcel.2019.07.029.
32. Zhao, L., Birdwell, L.D., Wu, A., Elliott, R., Rose, K.M., Phillips, J.M., Li, Y., Grinspan, J., Silverman, R.H., and Weiss, S.R. (2013). Cell-type-specific activation of the oligoadenylate synthetase-RNase L pathway by a murine coronavirus. J. Virol. *87*, 8408–8418. https://doi.org/10.1128/JVI.00769-13.
33. COVID-19 Host Genetics Initiative (2021). Mapping the human genetic architecture of COVID-19. Nature *600*, 472–477. https://doi.org/10.1038/s41586-021-03767-x.
34. COVID-19 Host Genetics Initiative (2022). A first update on mapping the human genetic architecture of COVID-19. Nature *608*, E1–E10. https://doi.org/10.1038/s41586-022-04826-7.
35. COVID-19 Host Genetics Initiative (2023). A second update on mapping the human genetic architecture of COVID-19. Nature *621*, E7–E26. https://doi.org/10.1038/s41586-023-06355-3.
36. Pairo-Castineira, E., Clohisey, S., Klaric, L., Bretherick, A.D., Rawlik, K., Pasko, D., Walker, S., Parkinson, N., Fourman, M.H., Russell, C.D., et al. (2021). Genetic mechanisms of critical illness in COVID-19. Nature *591*, 92–98. https://doi.org/10.1038/s41586-020-03065-y.
37. Bonnevie-Nielsen, V., Field, L.L., Lu, S., Zheng, D.-J., Li, M., Martensen, P.M., Nielsen, T.B., Beck-Nielsen, H., Lau, Y.-L., and Pociot, F. (2005). Variation in antiviral 2',5'-oligoadenylate synthetase (2'5'AS) enzyme activity is controlled by a single-nucleotide polymorphism at a splice-acceptor site in the OAS1 gene. Am. J. Hum. Genet. *76*, 623–633. https://doi.org/10.1086/429391.
38. Zhou, S., Butler-Laporte, G., Nakanishi, T., Morrison, D.R., Afilalo, J., Afilalo, M., Laurent, L., Pietzner, M., Kerrison, N., Zhao, K., et al. (2021). A Neanderthal OAS1 isoform protects individuals of European ancestry against COVID-19 susceptibility and severity. Nat. Med. *27*, 659–667. https://doi.org/10.1038/s41591-021-01281-1.
39. Mendez, F.L., Watkins, J.C., and Hammer, M.F. (2013). Neandertal origin of genetic variation at the cluster of OAS immunity genes. Mol. Biol. Evol. *30*, 798–801. https://doi.org/10.1093/molbev/mst004.
40. Wickenhagen, A., Sugrue, E., Lytras, S., Kuchi, S., Noerenberg, M., Turnbull, M.L., Loney, C., Herder, V., Allan, J., Jarmson, I., et al. (2021). A prenylated dsRNA sensor protects against severe COVID-19. Science *374*, eabj3624. https://doi.org/10.1126/science.abj3624.
41. Huffman, J.E., Butler-Laporte, G., Khan, A., Pairo-Castineira, E., Drivas, T.G., Peloso, G.M., Nakanishi, T., COVID-19 Host Genetics Initiative, Ganna, A., Verma, A., et al. (2022). Multi-ancestry fine mapping implicates OAS1 splicing in risk of severe COVID-19. Nat. Genet. *54*, 125–127. https://doi.org/10.1038/s41588-021-00996-8.
42. Banday, A.R., Stanifer, M.L., Florez-Vargas, O., Onabajo, O.O., Papenberg, B.W., Zahoor, M.A., Mirabello, L., Ring, T.J., Lee, C.-H., Albert, P.S., et al. (2022). Genetic regulation of OAS1 nonsense-mediated decay underlies association with COVID-19 hospitalization in patients of European and African ancestries. Nat. Genet. *54*, 1103–1116. https://doi.org/10.1038/s41588-022-01113-z.

43. Lee, D., Le Pen, J., Yatim, A., Dong, B., Aquino, Y., Ogishi, M., Pescarmona, R., Talouarn, E., Rinchai, D., Zhang, P., et al. (2023). Inborn errors of OAS-RNase L in SARS-CoV-2-related multisystem inflammatory syndrome in children. Science *379*, eabo3627. https://doi.org/10.1126/science.abo3627.

44. Ahrenfeldt, L.J., Otavova, M., Christensen, K., and Lindahl-Jacobsen, R. (2021). Sex and age differences in COVID-19 mortality in Europe. Wien. Klin. Wochenschr. *133*, 393–398. https://doi.org/10.1007/s00508-020-01793-9.

45. Qi, S., Ngwa, C., Morales Scheihing, D.A., Al Mamun, A., Ahnstedt, H.W., Finger, C.E., Colpo, G.D., Sharmeen, R., Kim, Y., Choi, H.A., et al. (2021). Sex differences in the immune response to acute COVID-19 respiratory tract infection. Biol. Sex Differ. *12*, 66. https://doi.org/10.1186/s13293-021-00410-2.

46. Li, Y., Banerjee, S., Wang, Y., Goldstein, S.A., Dong, B., Gaughan, C., Silverman, R.H., and Weiss, S.R. (2016). Activation of RNase L is dependent on OAS3 expression during infection with diverse human viruses. Proc. Natl. Acad. Sci. USA *113*, 2241–2246. https://doi.org/10.1073/pnas.1519657113.

47. Li, Y., Dong, B., Wei, Z., Silverman, R.H., and Weiss, S.R. (2019). Activation of RNase L in Egyptian Rousette Bat-Derived RoNi/7 Cells Is Dependent Primarily on OAS3 and Independent of MAVS Signaling. mBio *10*, e02414-19. https://doi.org/10.1128/mBio.02414-19.

48. Briggs, S., Blomqvist, E.K., Cuellar, A., Correa, D., and Burke, J.M. (2025). Condensation of human OAS proteins initiates diverse antiviral activities in response to West Nile virus. Genes Dev. *39*, 1162–1181. https://doi.org/10.1101/gad.352725.125.

49. Danziger, O., Patel, R.S., DeGrace, E.J., Rosen, M.R., and Rosenberg, B.R. (2022). Inducible CRISPR activation screen for interferon-stimulated genes identifies OAS1 as a SARS-CoV-2 restriction factor. PLoS Pathog. *18*, e1010464. https://doi.org/10.1371/journal.ppat.1010464.

50. Harioudh, M.K., Perez, J., Chong, Z., Nair, S., So, L., McCormick, K.D., Ghosh, A., Shao, L., Srivastava, R., Soveg, F., et al. (2024). Oligoadenylate synthetase 1 displays dual antiviral mechanisms in driving translational shutdown and protecting interferon production. Immunity *57*, 446–461.e7. https://doi.org/10.1016/j.immuni.2024.02.002.

51. Soveg, F.W., Schwerk, J., Gokhale, N.S., Cerosaletti, K., Smith, J.R., Pairo-Castineira, E., Kell, A.M., Forero, A., Zaver, S.A., Esser-Nobis, K., et al. (2021). Endomembrane targeting of human OAS1 p46 augments antiviral activity. eLife *10*, e71047. https://doi.org/10.7554/eLife.71047.

52. Wong, L.-Y.R., Zheng, J., Wilhelmsen, K., Li, K., Ortiz, M.E., Schnicker, N.J., Thurman, A., Pezzulo, A.A., Szachowicz, P.J., Li, P., et al. (2022). Eicosanoid signalling blockade protects middle-aged mice from severe COVID-19. Nature *605*, 146–151. https://doi.org/10.1038/s41586-022-04630-3.

53. Davis, M.A., Voss, K., Turnbull, J.B., Gustin, A.T., Knoll, M., Muruato, A., Hsiang, T.-Y., Dinnon Iii, K.H., Leist, S.R., Nickel, K., et al. (2022). A C57BL/6 Mouse Model of SARS-CoV-2 Infection Recapitulates Age- and Sex-Based Differences in Human COVID-19 Disease and Recovery. Vaccines (Basel) *11*, 47. https://doi.org/10.3390/vaccines11010047.

54. Rath, S., Prangley, E., Donovan, J., Demarest, K., Wingreen, N.S., Meir, Y., and Korennykh, A. (2019). Concerted 2-5A-Mediated mRNA Decay and Transcription Reprogram Protein Synthesis in the dsRNA Response. Mol. Cell *75*, 1218–1228.e6. https://doi.org/10.1016/j.molcel.2019.07.027.

55. Mao, X., Tokamov, S., Pahmeier, F., Lari, A., Xu, J., Harris, E., and Glaunsinger, B. (2025). Cytoplasmic mRNA decay by the anti-viral nuclease RNase L promotes transcriptional repression. Preprint at bioRxiv. https://doi.org/10.1101/2025.07.08.663778.

56. Burke, J.M., Gilchrist, A.R., Sawyer, S.L., and Parker, R. (2021). RNase L limits host and viral protein synthesis via inhibition of mRNA export. Sci. Adv. *7*, eabh2479. https://doi.org/10.1126/sciadv.abh2479.

57. Watkins, J.M., Douglas, C.J., Cusic, R., Seath, C.P., and Burke, J.M. (2025). RNase L regulates the antiviral proteome by accelerating mRNA decay, inhibiting nuclear mRNA export, and repressing RNAPII-mediated transcription. Preprint at bioRxiv. https://doi.org/10.1101/2025.07.18.665572.

58. Di, H., Elbahesh, H., and Brinton, M.A. (2020). Characteristics of Human OAS1 Isoform Proteins. Viruses *12*, 152. https://doi.org/10.3390/v12020152.

59. Harioudh, M.K., Perez, J., So, L., Maheshwari, M., Ebert, T.S., Hornung, V., Savan, R., Rouf Banday, A., Diamond, M.S., Rathinam, V.A., and Sarkar, S.N. (2024). The canonical antiviral protein oligoadenylate synthetase 1 elicits antibacterial functions by enhancing IRF1 translation. Immunity *57*, 1812–1827.e7. https://doi.org/10.1016/j.immuni.2024.06.003.

60. Sneller, M.C., Liang, C.J., Marques, A.R., Chung, J.Y., Shanbhag, S.M., Fontana, J.R., Raza, H., Okeke, O., Dewar, R.L., Higgins, B.P., et al. (2022). A Longitudinal Study of COVID-19 Sequelae and Immunity: Baseline Findings. Ann. Intern. Med. *175*, 969–979. https://doi.org/10.7326/M21-4905.

61. Vanderheiden, A., and Klein, R.S. (2022). Neuroinflammation and COVID-19. Curr. Opin. Neurobiol. *76*, 102608. https://doi.org/10.1016/j.conb.2022.102608.

62. Lee, W.-B., Choi, W.Y., Lee, D.-H., Shim, H., Kim-Ha, J., and Kim, Y.-J. (2019). OAS1 and OAS3 negatively regulate the expression of chemokines and interferon-responsive genes in human macrophages. BMB Rep. *52*, 133–138. https://doi.org/10.5483/BMBRep.2019.52.2.129.

63. Channappanavar, R., Fett, C., Mack, M., Ten Eyck, P.P., Meyerholz, D.K., and Perlman, S. (2017). Sex-Based Differences in Susceptibility to Severe Acute Respiratory Syndrome Coronavirus Infection. J. Immunol. *198*, 4046–4053. https://doi.org/10.4049/jimmunol.1601896.

64. Wang, L., Guzman, M., Muñoz-Santos, D., Honrubia, J.M., Ripoll-Gomez, J., Delgado, R., Sola, I., Enjuanes, L., and Zuñiga, S. (2023). Cell type dependent stability and virulence of a recombinant SARS-CoV-2, and engineering of a propagation deficient RNA replicon to analyze virus RNA synthesis. Front. Cell. Infect. Microbiol. *13*, 1268227. https://doi.org/10.3389/fcimb.2023.1268227.

65. Chiem, K., Martinez-Sobrido, L., Nogales, A., and DeDiego, M.L. (2021). Amino Acid Residues Involved in Inhibition of Host Gene Expression by Influenza A/Brevig Mission/1/1918 PA-X. Microorganisms *9*, 1109. https://doi.org/10.3390/microorganisms9051109.

66. Chiem, K., López-García, D., Ortego, J., Martinez-Sobrido, L., DeDiego, M.L., and Nogales, A. (2022). Identification of Amino Acid Residues Required for Inhibition of Host Gene Expression by Influenza Virus A/Viet Nam/1203/2004 H5N1 PA-X. J. Virol. *96*, e0040821. https://doi.org/10.1128/JVI.00408-21.

67. Schwarz, J.M., Rödelsperger, C., Schuelke, M., and Seelow, D. (2010). MutationTaster evaluates disease-causing potential of sequence alterations. Nat. Methods *7*, 575–576. https://doi.org/10.1038/nmeth0810-575.

68. Goddard, T.D., Huang, C.C., Meng, E.C., Pettersen, E.F., Couch, G.S., Morris, J.H., and Ferrin, T.E. (2018). UCSF ChimeraX: Meeting modern challenges in visualization and analysis. Protein Sci. *27*, 14–25. https://doi.org/10.1002/pro.3235.

69. Jumper, J., Evans, R., Pritzel, A., Green, T., Figurnov, M., Ronneberger, O., Tunyasuvunakool, K., Bates, R., Žídek, A., Potapenko, A., et al. (2021). Highly accurate protein structure prediction with AlphaFold. Nature *596*, 583–589. https://doi.org/10.1038/s41586-021-03819-2.

70. Saiz, M.L., DeDiego, M.L., López-García, D., Corte-Iglesias, V., Baragaño Raneros, A., Astola, I., Asensi, V., López-Larrea, C., and Suarez-Alvarez, B. (2021). Epigenetic targeting of the ACE2 and NRP1 viral receptors limits SARS-CoV-2 infectivity. Clin. Epigenetics *13*, 187. https://doi.org/10.1186/s13148-021-01168-5.

71. Sánchez-Tacuba, L., Rojas, M., Arias, C.F., and López, S. (2015). Rotavirus Controls Activation of the 2'-5'-Oligoadenylate Synthetase/RNase L Pathway Using at Least Two Distinct Mechanisms. J. Virol. *89*, 12145–12153. https://doi.org/10.1128/JVI.01874-15.

72. Toptan, T., Hoehl, S., Westhaus, S., Bojkova, D., Berger, A., Rotter, B., Hoffmeier, K., Cinatl, J., Ciesek, S., and Widera, M. (2020). Optimized qRT-PCR Approach for the Detection of Intra- and Extra-Cellular SARS-CoV-2 RNAs. Int. J. Mol. Sci. *21*, 4396. https://doi.org/10.3390/ijms21124396.

73. Alexandersen, S., Chamings, A., and Bhatta, T.R. (2020). SARS-CoV-2 genomic and subgenomic RNAs in diagnostic samples are not an indicator of active replication. Nat. Commun. *11*, 6059. https://doi.org/10.1038/s41467-020-19883-7.

74. Yu, Y.-R.A., O'Koren, E.G., Hotten, D.F., Kan, M.J., Kopin, D., Nelson, E.R., Que, L., and Gunn, M.D. (2016). A Protocol for the Comprehensive Flow Cytometric Analysis of Immune Cells in Normal and Inflamed Murine Non-Lymphoid Tissues. PLoS One *11*, e0150606. https://doi.org/10.1371/journal.pone.0150606.

75. Schmidt, E.K., Clavarino, G., Ceppi, M., and Pierre, P. (2009). SUnSET, a nonradioactive method to monitor protein synthesis. Nat. Methods *6*, 275–277. https://doi.org/10.1038/nmeth.1314.

76. Goodman, C.A., Mabrey, D.M., Frey, J.W., Miu, M.H., Schmidt, E.K., Pierre, P., and Hornberger, T.A. (2011). Novel insights into the regulation of skeletal muscle protein synthesis as revealed by a new nonradioactive in vivo technique. FASEB J. *25*, 1028–1039. https://doi.org/10.1096/fj.10-168799.

77. Ewels, P., Magnusson, M., Lundin, S., and Käller, M. (2016). MultiQC: summarize analysis results for multiple tools and samples in a single report. Bioinformatics *32*, 3047–3048. https://doi.org/10.1093/bioinformatics/btw354.

78. Ioannidis, N.M., Rothstein, J.H., Pejaver, V., Middha, S., McDonnell, S.K., Baheti, S., Musolf, A., Li, Q., Holzinger, E., Karyadi, D., et al. (2016). REVEL: An Ensemble Method for Predicting the Pathogenicity of Rare Missense Variants. Am. J. Hum. Genet. *99*, 877–885. https://doi.org/10.1016/j.ajhg.2016.08.016.

79. Ng, P.C., and Henikoff, S. (2001). Predicting deleterious amino acid substitutions. Genome Res. *11*, 863–874. https://doi.org/10.1101/gr.176601.

80. Adzhubei, I.A., Schmidt, S., Peshkin, L., Ramensky, V.E., Gerasimova, A., Bork, P., Kondrashov, A.S., and Sunyaev, S.R. (2010). A method and server for predicting damaging missense mutations. Nat. Methods *7*, 248–249. https://doi.org/10.1038/nmeth0410-248.

81. Kircher, M., Witten, D.M., Jain, P., O'Roak, B.J., Cooper, G.M., and Shendure, J. (2014). A general framework for estimating the relative pathogenicity of human genetic variants. Nat. Genet. *46*, 310–315. https://doi.org/10.1038/ng.2892.

STAR★METHODS

KEY RESOURCES TABLE

REAGENT or RESOURCE	SOURCE	IDENTIFIER
Antibodies		
Mouse monoclonal anti-*c*-myc	Thermo Fisher Scientific	Cat#MA1-980; RRID:AB_558470
Mouse monoclonal anti-actin	Sigma-Aldrich	Cat#A1978; RRID:AB_476692
Rabbit monoclonal anti-OAS1	Cell Signaling	Cat#14498; RRID:AB_2798498
Rabbit polyclonal anti-OAS3	Abcam	Cat#ab154270; RRID:AB_3106889
Rat monoclonal anti-CD16/CD32	BD BioSciences	Cat#553145; RRID:AB_394660
Rat monoclonal anti-CD11b conjugated to brilliant violet 650	Biolegend	Cat#101239; RRID:AB_11125575
Rat monoclonal anti-MHCII (IA/IE) conjugated to brilliant violet 711	Biolegend	Cat#107643, RRID:AB_2565976
Armenian hamster monoclonal anti-CD69 conjugated to FITC	Biolegend	Cat#104506; RRID:AB_313109
Rat monoclonal anti-Ly6C conjugated to PerCP-Cy5.5	Biolegend	Cat#128012; RRID:AB_1659241
Rat monoclonal anti-CD3 conjugated to PE	BD BioSciences	Cat#555275; RRID:AB_395699
Mouse monoclonal anti-CD64 conjugated to PE/Cy7	Biolegend	Cat#139314; RRID:AB_2563904
Armenian hamster monoclonal anti-CD11c conjugated to APC	eBioSciences	Cat#17-0114-82; RRID:AB_469346
Rat monoclonal anti-Ly6G conjugated to Alexa Fluor 700	Biolegend	Cat#127622, RRID:AB_10643269
Rat monoclonal anti-CD45 conjugated to APC-eFluor 780	eBioSciences	47-0451-82, RRID:AB_1548781
Mouse monoclonal anti-puromycin	Sigma-Aldrich	Cat# MABE343; RRID:AB_2566826
Mouse monoclonal anti-GAPDH conjugated to horseradish peroxidase	Abcam	Cat#ab9484; RRID:AB_307272
Mouse monoclonal anti-GST conjugated to horseradish peroxidase	Thermo Fisher Scientific	Cat# MA4-004-HRP; RRID:AB_2537634
Anti- AMP^2/GMP^2	Bellbrook Labs	Cat# 2247
Goat anti-rabbit polyclonal antibody conjugated to horseradish peroxidase	Millipore	Cat#12–348; RRID:AB_390191
Goat anti-mouse polyclonal antibody conjugated to horseradish peroxidase	Millipore	Cat#12–349; RRID:AB_390192
Bacterial and virus strains		
Viral strain: SARS-CoV-2-MAD6	Laboratory of Luis Enjuanes (CNB-CSIC) (Wang et al.[64])	N/A
Viral strain: A mouse-adapted SARS-CoV-2, adapted to grow in mice (SARS-CoV-2-MA)	Laboratory of Luis Enjuanes (CNB-CSIC) (Wong et al.[52])	N/A
Retroviral vector expressing hACE2	Laboratory of Pablo Gastaminza (CNB-CSIC)	N/A
Bacterial *E. coli* strain BL21 (DE3)	Thermo Fisher Scientific	Cat#C600003
Bacterial *E. coli* strain DH5α	Thermo Fisher Scientific	Cat#18258012
Biological samples		
PBMCs	From human patients	N/A
Chemicals, peptides, and recombinant proteins		
Puromycin	InVivoGen	Cat#ant-pr-1
Lipofectamine 3000	Thermo Fisher Scientific	Cat#L3000015
Lipofectamine RNAiMax	Thermo Fisher Scientific	Cat#13778075
blasticidin	Thermo Fisher Scientific	Cat#J67216.XF

(*Continued on next page*)

Continued

REAGENT or RESOURCE	SOURCE	IDENTIFIER
polyinosinic:polycytidylic acid (poly(I:C))	InVivoGen	Cat# tlrl-pic
High-Capacity cDNA transcription kit	Thermo Fisher Scientific	Cat#4374966
SuperSignal West femto maximum sensitivity substrate	Thermo Fisher Scientific	Cat# 34095
Live/dead Aqua cell stain	Thermo Fisher Scientific	Cat#L34957
Brilliant Violet Stain Buffer	BD Biosciences	Cat# 563794
Recombinant OAS1-p42 protein	Bellbrook Labs	N/A
Recombinant OAS1-p46 protein	This paper	N/A
Recombinant OAS1-p46-K206Q protein	This paper	N/A
Critical commercial assays		
Ccl2 ELISA assay	Invitrogen	Cat#88-7391
AMP the Transcreener® AMP^2 Fluorescent Polarization (FP) assay	Bellbrook Labs	Cat#3027-1K
Deposited data		
European Genome-Phenome Archive	This paper	EGAD50000000094
Experimental models: cell lines		
Human A549	ATCC	CCL-185
Human HEK293T	ATCC	CRL-11268
Vero E6	Laboratory of Luis Enjuanes (CNB-CSIC)	N/A
Vero-TMPRSS2	Laboratory of Luis Enjuanes (CNB-CSIC)	N/A
Experimental models: organisms/strains		
C57BL/6N-$Oas3^{em1(IMPC)bay}$	Baylor College of Medicine (Houston, TX)	RRID:MMRRC_066927-MU
Oligonucleotides		
Primers to generate plasmids px330, to generate OAS3 KO cells, with sgRNA guide 1: 5′- CACCG cagtgagatgcgggcatcgc- 3′ and 3′- C gtcactctacgcccgtagcg CAAA-5′	This paper	N/A
Primers to generate plasmids px330, to generate OAS3 KO cells, with sgRNA guide 2: 5′- CACCG agagaaggcgcggc gcgctc-3′and 3′- C tctcttccgcg ccgcgcgag CAAA-5′	This paper	N/A
Knock-down experiments: siRNA for OAS1	Thermo Fisher Scientific	Cat#s511
Knock-down experiments: siRNA for OAS3	Thermo Fisher Scientific	Cat#s9797
Knock-down experiments: non-targeting (NT) negative control siRNA	Thermo Fisher Scientific	Cat# AM4635
qPCR: human *IFNL1* (Hs00601677_g1), human *TNF* (Hs00174128_m1), human *CXCL10* (Hs00171042_m1), human *CCL2* (Hs00234140_m1), human *IL6* (Hs 00174131_m1), human *OAS1* (Hs00973635_m1), human *OAS3* (Hs00196324_m1), human *GAPDH* (Hs02786624_g1)	Thermo Fisher Scientific	Cat#4331182
qPCR: murine *Ccl2* (Mm00441242_m1), murine *Cxcl10* (Mm00445235_m1), murine *Tnf* (Mm00443258_m1), murine *Ccl8* (Mm01297183_m1), murine *Oas3* (Mm00460944_m1), murine *Hprt1* (Mm00446968_m1)	Thermo Fisher Scientific	Cat#4331182

(*Continued on next page*)

Continued

REAGENT or RESOURCE	SOURCE	IDENTIFIER
Primers to analyze viral replication, by qPCR: SARS-2-RdRp-15431-VS (5′-GTGAAATGGTCATGTGTGGCGG-3′) and SARS-2RdRp-15530-RS (5′- CAAATGTTAAAAACACTATTAGCATA-3′)	This paper	N/A
Primers to analyze viral transcription, by qPCR: SARS-2-leader-VS (5′- TCCCAGGTAACAAACCAACCAACT-3′) and SARS-2-7a-RS (5′-AAATGG TGAATTGCCCTCGT-3′)	This paper	N/A
Primers to analyze GAPDH expression by qPCR: 5′-TGCCATGGGTGGAATCA TATTGGA-3′ (sense) and 5′-TCGGA GTCAACGGATTTGGGTCGT-3 (antisense)	This paper	N/A
Recombinant DNA		
pCR-XL-2-TOPO plasmid	Thermo Fisher Scientific	Cat#K8040-20
pCAGGS plasmid	Lab Luis Martínez-Sobrido (Chiem et al.[65]; Chiem et al;[66])	N/A
pcDNA3.1 plasmid	Thermo Fisher Scientific	Cat# V79020
Modified px330 plasmid	Lab Pedro Antonio Mateos-Gómez	N/A
pGEX-6P-2 plasmid	NovoPro	Cat#V010911
Software and algorithms		
ImageJ software	N/A	https://imagej.nih.gov/ij/
FacsDiva software, version 5	BD Biosciences	https://www.bdbiosciences.com/
FlowJo software, version 10	FlowJo LLC	https://www.flowjo.com/
GraphPad Prism software, version 9.3.1	GraphPad Software	https://www.graphpad.com
Geneious	Dotmatics	https://www.geneious.com/
AlphaFold	Google DeepMind and Isomorphic labs	https://alphafoldserver.com/welcome
R	R-project	https://www.r-project.org/
Pandas (Python library)	N/A	https://pandas.pydata.org/
Statsmodels (Python library)	N/A	https://www.statsmodels.org/stable/index.html
Matplot (Python library)	N/A	https://matplotlib.org/
Seaborn (Python library)	N/A	https://seaborn.pydata.org/
SKAT (R package)	N/A	https://cran.r-project.org/web/packages/SKAT/index.html
Hardy-Weinberg equilibrium (R package)	N/A	https://cran.r-project.org/web/packages/HardyWeinberg/index.html
PyMol	Schrodinger	https://www.pymol.org/2/
ChimeraX	UCSF	https://www.cgl.ucsf.edu/chimera/
Bcl2fastq2	Illumina	https://support.illumina.com/sequencing/sequencing_software/bcl2fastq-conversion-software.html
FastQC	Babrahan Bioinformatics	https://www.bioinformatics.babraham.ac.uk/projects/fastqc/
MultiQC	Seqera	https://seqera.io/multiqc/
BWA-MEM	N/A	https://github.com/lh3/bwa
GATK	Broad Institute	https://gatk.broadinstitute.org/hc/en-us
VEP	Ensembl	https://useast.ensembl.org/info/docs/tools/vep/index.html
SIFT	N/A	https://sift.bii.a-star.edu.sg/index.html
PolyPhen-2	N/A	http://genetics.bwh.harvard.edu/pph2/

(*Continued on next page*)

Continued

REAGENT or RESOURCE	SOURCE	IDENTIFIER
CADD	University of Washington	https://cadd.gs.washington.edu/
MutationTaster	Schwarz et al.[67]	https://www.mutationtaster.org/
Analysis pipeline	This paper	https://doi.org/10.5281/zenodo.17396248
Other		
TOPO-XL cloning system	Invitrogen	Cat#K8050-10

EXPERIMENTAL MODEL AND STUDY PARTICIPANT DETAILS

Human subjects and ethics

We studied patients (n = 342) who suffered SARS-CoV-2 infection in Spain, as confirmed by PCR or an antigen test, within the period comprised between March 2020 and March 2021, i.e., before vaccines became available in this country. The study is part of the Inmungen-CoV2 project approved by the Ethics Committee (CEIm) of Hospital Clinic of Barcelona (HCB) (Reg.HCB/2020/0357) and the Ethics Committee of CSIC (049/2020). Age and certain diseases are risk factors for severe COVID-19 that could have confounding effects in the search for genetic factors. For this reason, we selected COVID-19 patients of age comprised between 18 and 65 years. We excluded patients with cancer, chronic lung or heart diseases, patients with organ transplants or with other active viral infections, such as VIH. The core group of this study were patients hospitalized in the Hospital Clinic of Barcelona, from which we have epidemiological and clinical data. Blood samples were obtained from patients of this hospital who provided written consent to participate in the Inmungene-CoV2 study or were obtained from the COVIDBANK of HCB-IDIBAPS Biobank. In addition, we collected blood samples from the following hospitals in Spain: Hospital Universitari Vall d'Hebron (Barcelona), Hospital Universitari Mútua de Terrassa (Terrasa, Barcelona), Hospital Universitario Central de Asturias, Hospital Clínico Universitario de Valladolid, and the biobanks from Hospital General de Alicante, Hospital Universitari i Politènic La Fe, Hospital Clínic Universitari de València and the Public Health Biobanc from FISABIO. Recruitment of patients was approved by each of the corresponding ethics committees. The study conformed to the principles set out in the World Medical Association (WMA) Declaration of Helsinki. Some features of the patients are described below:

P1: 47-year-old man devoid of any relevant clinical history who suffered severe COVID-19 requiring ICU.

P2: woman aged 39, who had severe COVID-19 required ICU admission due to high oxygen needs. She had severe lymphocytopenia (0.3×10^9/L) and neutrophilia ($10.7*10^9$/L) and moderate inflammatory parameters (CRP = 9.62 mg/dL; ferritin = 370 ng/mL; D-dimer = 900 ng/mL) receiving corticosteroids and anti-IL6 (Sarilumab).

P3: pregnant (10 weeks) woman, aged 31, presented with mild COVID-19. She was hospitalized for 3 days.

P4: 61-year-old man. After being admitted to hospital for COVID-19, he experienced clinical worsening, showed reduced lymphocytes (0.9×10^9/L) and strong inflammatory biochemical parameters reaching high values (CRP = 6.99 mg/dL; ferritin = 2,237 ng/mL; D-dimer = 800 ng/mL) that responded to treatment with anti-IL6 (tocilizumab) and did not require ICU.

P5: 36-year-old man. He spent five days in the hospital, during which he exhibited mild COVID-19 pneumonia without need for oxygen.

P6: asymptomatic young woman, aged 25, positive for SARS-CoV-2.

P7: 37-year-old man who suffered severe COVID-19 with hypoxemia requiring ICU admission. Lymphocytes were in the low normal range (1.2×10^9/L), but with a reduced proportion of $CD8^+$ T cells, and he developed hyperinflammation (CRP = 7.17 mg/dL; ferritin = 967 ng/mL; D-dimer = 500 ng/mL) that responded to tocilizumab.

P8: woman aged 62. She suffered severe COVID-19 being admitted to ICU for hypoxemia and developing severe lymphocytopenia (0.4×10^9/L). She showed two waves of hyperinflammation before and after ICU admission, reaching high values of inflammatory markers (CRP = 22.2 mg/dL; ferritin = 813 ng/mL; D-dimer = 2,300) and receiving corticosteroids.

P9: man, aged 48 and devoid of any relevant clinical history. He showed COVID-19 of moderate severity requiring oxygen mask and accompanied by low lymphocytes and a strong inflammatory reaction (CRP >7 mg/dL; ferritin >1,000 ng/mL; D-dimer from 400 to 1,800 ng/mL). Hyperinflammation was responsive to treatment with corticosteroids.

P10: man, aged 49, devoid of any relevant clinical history. He showed COVID-19 of moderate severity requiring oxygen mask and treatment with tocilizumab.

P11: man, aged 47, hospitalized with mild COVID-19 symptoms.

P12: man, aged 62, hospitalized with mild COVID-19 symptoms.

P13: woman, aged 40. She was hospitalized with mild COVID-19symptoms.

P14: pregnant woman, aged 35. Asymptomatic, COVID-19 was casually detected when tested before delivery.

P15: man, aged 60. He was hospitalized with COVID-19, presenting a strong inflammatory reaction (CRP >7 mg/dL; ferritin>1,000 ng/mL; D-dimer>400 ng/mL). He received IL-1 inhibitor (anakinra).

P16: 32-year-old man hospitalized with mild COVID-19.

P17: man, aged 59, who had critical COVID-19 requiring ICU admission of long duration.

P18: man, aged 48, who had COVID-19 with moderate severity, showing inflammation (CRP = 6 mg/dL; high ferritin = 1,802 ng/mL, D-dimer = 2,000 ng/mL, and IL6 = 69 ng/mL), and clinical worsening; he received oxygen and corticosteroid treatment.
P19: man, aged 49, had milder COVID-19 with mild inflammation (CRP = 10.79 mg/dL; ferritin = 290 ng/mL; D-dimer = 900 ng/mL).
P20: 45 years-old-woman. She had mild COVID-19 that did not require hospitalization.
P21: man, aged 59, who had severe COVID-19 requiring ICU admission.
P22: man, aged 63, who had severe COVID-19 requiring ICU admission.
P23: man, aged 60, who had moderate COVID-19 with signs of inflammatory responses.
P24: man, aged 63, who showed mild COVID-19 symptoms.
P25: pregnant woman, aged 29. She was hospitalized with mild/moderate COVID-19.
P26: woman, aged 57, who was hospitalized showing mild/moderate COVID-19.
P27: woman, aged 39, who showed mild COVID-19 not requiring hospitalization.
P28: woman, aged 40, who showed mild COVID-19 not requiring hospitalization.
P29: man, aged 43, devoid of any previous relevant clinical history, showed COVID-19 of moderate severity accompanied by low lymphocyte counts and inflammatory markers with high IL-6 (169 ng/mL), responsive to tocilizumab.
P30: woman, aged 45, hospitalized with mild COVID-19 without requirements of oxygen support.

Animal studies and ethics

Mice with gene and allele *Oas3* em1(IMPC)Bay (RRID:MMRRC_066927-MU) in the C57BL/6 background were obtained from the Baylor College of Medicine (Houston, TX) and maintained by the Knockout Mouse Phenotyping Project (KOMP2). Then, mice were maintained in heterozygosis at the animal house of the School of Medicine and School of Psychology of the University of Barcelona (UB) under controlled environmental conditions with free access to food and water. We used adult young (2.5–4.5 months) male and female $Oas3^{-/-}$ (n = 96) and $Oas3^{+/+}$ (n = 95) littermate mice. Animal work was conducted in strict accordance with EU guidelines 2010/63/UE about the protection of animals used for experimentation and the Spanish Animal Welfare Act 32/2007, and in compliance with the NIH Guide for the Care and Use of Laboratory Animals. All experiments were conducted with the approval of the Ethical Committee of UB (CEEA) and the local regulatory bodies of the *Generalitat de Catalunya*, or the Ethical Review Committee of the *Centro de Investigación en Sanidad Animal* (CISA-INIA, CSIC) and *Comunidad de Madrid* (Permit number: PROEX 260.4). The work is reported following the ARRIVE guidelines (see supplemental information).

METHOD DETAILS

Whole exome sequencing

Whole Exome Sequencing (WES) was performed at two different sequencing centers. Half of the samples were sequenced at a commercial service, NIMGenetics (Madrid, Spain), whereas the other half were sequenced by the EASI-Genomics consortium. In both cases, the SureSelectXT Human All Exon v6 Capture Library (Agilent Technologies) was used to capture the coding region. The quality of the final libraries was assessed using the TapeStation (Agilent Technologies) and a Qubit fluorometer (Thermo Fisher Scientific). Based on Qubit quantification and sizing analysis, sequencing libraries were normalized and pooled in equimolar ratios. 150 (NIMGenetics) or 100 bp (EASI-Genomics) paired-end sequencing was performed using NovaSeq 6000 instruments (Illumina Inc.) using standard Illumina protocols (S2 and S4 flow cells). Using this protocol, we obtained around 41–42 million reads per sample, with more than 90% with a quality score of at least Q30 and a mean coverage of around 100x.

Structural modeling

We modeled the structural effect of the identified variants using the solved 3D structure of human OAS1 (PDB: 4IG8) and the first domain of OAS3 (PDB: 4SN3). We obtained the structure of domains II and III of OAS3 with Chimera[68] using the solved structures of OAS1 and the first OAS domain in OAS3. All variants were then modeled using Chimera followed by energy minimization. We compared our predicted structures with those available using AlphaFold[69] and concluded that the models were almost identical. We visualized the effect of the variants using PyMol (https://pymol.org/2/).

Alignment

The alignment was produced with CLUSTAL X implemented in the software Genious (Biomatters Ltd., https://www.geneious.com) using OAS1 (amino acids 1–367) and the three NTP-transferase+OAS domains in OAS3: OAS3-I (from amino acid 1 till 361), OAS3-II (400–740) and OAS3-III (745–1087). The parameters for the alignment were "Global alignment with free end gaps", a gap open penalty of 12, a gap extension penalty of 3 and with 2 refinement iterations, using the protein sequence for OAS1 (ENSP00000445409) and OAS3 (ESNP00000228928) although the latter was divided in its three domains that we refer to as OAS3-I from residue 1 to residue 361; OAS3-II from residue 400 to 740, and OAS3-III from 745 to 1087. The use of different parameters or aligners did not yield significantly different results.

Selection of variants to analyze their functional effect

The list of variants to be analyzed (Data S1) was obtai ned by a combination of the following criteria.

1. Genetic criteria (mandatory). Variants in *OAS1*, *OAS2* and *OAS3* with a coverage of at least 20x and with a quality value of at least Q20 were selected. Selection was restricted to missense variants as well as those affecting consensus acceptor and donor sequences for splicing.
2. The information provided by tools predicting pathogenicity (SIFT, PolyPhen2, CADD or MutationTaster). REVEL scores were also determined, although it is a rather conservative tool that combines the results from other 13 tools. It is included here for reference. For quantitative and qualitative predictions, we used SIFT and PolyPen2. We chose those variants not classified as tolerated (SIFT) or benign (PolyPhen2). For CADD, we chose those with a score over 15. Finally, the use of MutationTaster provided qualitative predictions.
3. We also considered the information derived from the structural modeling of the variants, prioritizing variants in residues apparently important for the maintenance of the 3D structure of the proteins or for the binding of dsRNA to the protein.

A similar strategy was used for variants from the COVID-19 Human Genetic Effort (CHGE, https://www.covidhge.com/) cohort. In this case, we decided to include variants that were found in regions not covered by variants identified in the Spanish cohort. In some cases, a variant was selected as it generated a different amino acid change in a variant position already found in the Spanish population. We also included ultra-rare or rare variants predicted to be neutral and with no evidence of pathogenicity as control variants. Finally, even though not fulfilling the inclusion criteria described above, we also analyzed apparently neutral variants when several variants were found in the same individual. According to these criteria, we generated the final list of variants to be analyzed in functional studies (Data S2).

Determining the phase of multiple *OAS* variants in the same individual

When more than one *OAS* variant appeared in the same individual, we determined whether they were in phase as this could have an impact on protein physiology. We cloned the PCR products obtained using the primers and PCR conditions stated in Table S1 into the pCR-XL-2-TOPO vector using a TA-cloning system (Topo-XL, Invitrogen) as per the manufacturer's instructions. Plasmid DNA was purified from overnight bacterial cultures grown at 37°C in LB medium, using a homemade alkaline lysis method (https://www2.clarku.edu/faculty/dlarochelle/miniprep_protocol.pdf) and 5–10 colonies were Sanger sequenced in both directions to identify whether the amplicons had the different variants in phase. All patients with rare variants in *OAS1* where homozygous for the A-allele in the rs10774671 SNV. Therefore, there was no need for determining phase between this polymorphism and the rare allele identified in this report.

Cell lines

Human lung epithelial carcinoma A549 (ATCC CCL-185, derived from lung carcinomatous tissue from a 58-year-old Caucassian male), human embryonic kidney HEK293T (ATCC CRL-11268, derived from a fetus), Vero E6 and Vero cells overexpressing the TMPRSS2 (Vero-TMPRSS2, kindly provided by Prof. Luis Enjuanes, CNB-CSIC, derived from the kidney of a normal adult African Green monkey) cells were grown in Dulbecco's modified Eagle's medium (DMEM; Mediatech, Inc.) containing 10% fetal bovine serum (FBS) and 2 mM L-glutamine at 37°C in a 5% CO_2 incubator.

Viruses and virus titrations

We used a SARS-CoV-2 strain isolated from Vero E6 cells, originated from a nasal swab from a patient infected in Madrid, Spain, at the beginning of 2020, termed SARS-CoV-2-MAD6 strain. This strain is similar to the B.1 variants and it was kindly provided by Prof. Luis Enjuanes, at Centro Nacional de Biotecnología, CNB-CSIC, Spain.[64] Viral stocks were grown in Vero E6 cells. A mouse-adapted SARS-CoV-2, adapted to grow in mice (SARS-CoV-2-MA),[52] kindly provided by Prof. Luis Enjuanes, was grown in the Vero-TMPRSS2 cells. SARS-CoV-2 and SARS-CoV-2-MA were titrated by plaque assay (PFU/mL) in confluent Vero E6 and Vero-TMPRSS2 cells, seeded in 24-well plates, respectively, as previously described.[70]

Plasmids

The OAS1 ORFs, encoding the p42 or the p46 isoforms, fused to an N-terminal c-myc epitope tag were cloned into the pCAGGS plasmid[65,66] using *Sac*I and *Sma*I restriction sites. To this end, OAS1 fragments fused to the c-myc and flanked by *Sac*I and *Sma*I restriction sites were synthesized by IDT DNA Inc (Iowa, USA), and cloned using standard techniques. The OAS3 ORF C-terminally fused to c-myc and 6xHis epitope tags was cloned in the pcDNA3.1 plasmid using *Hind*III and *Not*I restriction sites (Genscript). Plasmids encoding the different *OAS1* and *OAS3* variants were generated by obtaining PCR products using oligonucleotides encoding the nucleotide changes and the PCR products were subcloned in the plasmids encoding the wild-type (WT) proteins using unique restriction enzymes. Alternatively, the plasmids were generated by Genscript.

To generate *OAS3* KO cells, the best short guide RNAs (sgRNAs) to be used, were selected using the webpages (https://www.atum.bio/eCommerce/cas9/input?multipleContacts=false and http://crispor.tefor.net). The sgRNA sequences selected were: 5′-cagtgagatgcgggcatcgc-3′and 5′- agagaaggcgcggcgcgctc-3'. The cDNAs complementary to the two different sgRNAs were cloned in a modified pX330 plasmid (kindly provided by Dr. Pedro A. Mateos, Universidad de Alcalá de Henares, Spain), expressing the RNA guides under the U6 promoter and encoding the CAS9 gene, and modified to codify a gene encoding for resistance to puromycin. To this end, a pair of forward and reverse oligonucleotides for the generation of each sgRNA (synthesized by IDT) were

annealed and phosphorylated by incubating the forward and reverse primers with T4 polynucleotide kinase (New England Biolabs), during 30 min at 37°C, followed by 95°C during 5 min and then ramp down to 25°C, at 5 °C/min. The phosphorylated and annealed primers were inserted into plasmid vector pX330 between *Bbs*I restriction sites. *E.coli* (DH5α strain) bacteria were transformed with the plasmids and grown in LB medium at 37°C during 16 h. Plasmids were purified from the bacteria using the EZNA plasmid DNA mini kit (Omega Bio-tek).

Generation of A549 *OAS3* KO cells

To generate A549 *OAS3* KO cells, A549 cells (12-well plate format) were transfected with the pX330 plasmids (1,250 ng/well) expressing the sgRNAs, using lipofectamine 3000 (Thermo Fisher Scientific). At 24 hpt, cells were treated with 1 μg/mL of puromycin (InVivoGen) to select for plasmid-transfected cells. At 48 h after puromycin treatment, media was exchanged with fresh media without puromycin. Surviving cells were detached with trypsin and cloned three times by limiting dilution. Different clones were genotyped by Sanger sequencing (Macrogen) and analyzed by Western blot, as described below.

Overexpression of hACE-2 in A549 and HEK293T cells

To generate A549 and HEK293T cells susceptible to SARS-CoV-2 infection (A549-ACE2 and HEK293T-ACE2), HEK293T, A549-WT and A549- *OAS3* KO A549 cells (6-well plate format) were transduced with a retrovirus expressing the hACE-2 protein and a gene conferring resistance to the antibiotic blasticidin (kindly provided by Dr. Pablo Gastaminza, at Centro Nacional de Biotecnología, CNB-CSIC, Spain). The transduced cells were selected by growing the cells in the presence of 2.5 μg/mL blasticidin (Thermo Fisher Scientific).

Effect of OAS1 and OAS3 variants on RNA integrity

HEK293T-ACE2 (24-well plate format) were transiently co-transfected with 500 ng/well of pCAGGS plasmids encoding the *OAS1* or *OAS3* variants, or transfected with empty plasmid as internal control, using Lipofectamine 3000 (Thermo Fisher Scientific). For *OAS1*, we studied the effect of the rare variants on both rs10774671 common genotypes (A/A and G/G). At 24 h post-transfection (hpt), cells were treated with polyinosinic:polycytidylic acid (poly(I:C)) (InvivoGen), at 1 μg/mL for an additional 24 h or HEK293T-ACE2 cells were infected with SARS-CoV-2 at a multiplicity of infection (MOI) of 1, during 24 h. Alternatively, A549-ACE2 cells were transfected twice with siRNAs, as indicated below and 24 h after the second transfection, the cells were infected with SARS-CoV-2 (MOI 1). Total RNA was extracted using the Total RNA extraction kit (Omega Biotek) and the RNA integrity was analyzed in a Bioanalyzer 2100 (Agilent). The amount of the degradation bands was quantified by densitometry using the ImageJ software and normalized to the amount of the 18S rRNA within each sample, in a similar way as previously described.[71]

Effect of OAS1 and OAS3 variants on protein expression

HEK293T-ACE2 cells (12-well plate format) were transiently co-transfected, with 1,000 ng/well of pCAGGS plasmids encoding the *OAS1* (rs10774671 G/G or A/A genotypes) or *OAS3* variants, or transfected with empty plasmid as internal control, using Lipofectamine 3000 (Thermo Fisher Scientific). At 24 and 48 hpt, the cells were lysed in passive lysis buffer (Promega) and clarified by centrifugation.

siRNA-mediated silencing

Human A549-ACE2 cells (24 or 96-well plate format) were transfected independently with different "silencer select" small interfering RNAs (siRNAs) specific for human *OAS1* and *OAS3* genes (ThermoFisher Scientific, s511 and s9797, respectively), or with the non-targeting (NT) negative control siRNA (ThermoFisher Scientific, AM4635). All siRNAs were transfected, using lipofectamine RNAiMax (ThermoFisher Scientific), at a final concentration of 20 nM, according to the manufacturer's instructions. The siRNAs were transfected twice, 24 h apart.

Western blot

Cell lysates were mixed with Laemmli sample buffer containing 2.5% β-mercaptoethanol, and heated at 95°C for 5 min, before SDS-PAGE electrophoresis. Proteins were transferred to nitrocellulose membranes (Biorad), and detected using mouse monoclonal antibodies specific for the c-myc epitope tag (Thermo Fisher Scientific MA1—980, RRID:AB_558470), and the human actin (Sigma-Aldrich A1978, RRID:AB_476692), a rabbit monoclonal antibody specific for OAS1 (Cell Signaling 14498, RRID:AB_2798498), and a rabbit polyclonal antibody specific for OAS3 (Abcam ab154270, RRID:AB_3106889), all of them at a 1:1000 dilution. Later on, the membranes were incubated with a 1:4,000 dilution of goat anti-rabbit (pAb) or 1:2,000 dilution of goat anti-mouse (mAb) IgG antibodies conjugated to horseradish peroxidase (Millipore 12–348, RRID:AB_390191 and Millipore 12–349, Millipore Cat# 12–349, RRID:AB_390192, respectively), and membranes were revealed by chemiluminescence using the SuperSignal west femto maximum sensitivity substrate (ThermoFisher Scientific).

Effect of OAS1 and OAS3 variants on innate immune responses

A549 *OAS3* KO cells (24-well plate format) were transiently co-transfected, with 500 ng/well of pCAGGS plasmids encoding the *OAS1* (rs10774671 G/G or A/A genotypes) or *OAS3* variants, or transfected with empty plasmid as internal control, using

Lipofectamine 3000 (Thermo Fisher Scientific). At 24 hpt, cells were transfected with poly(I:C), at 1 μg/mL for an additional 24 h. A549-ACE2 *OAS3* KO cells (24-well plate format) and parental cells were transfected with poly(I:C), at 50 or 250 ng/mL for 24 h. A549-ACE2 cells were transfected with poly(I:C), at 50 or 250 ng/mL for 24 h. Total RNA was extracted using the Total RNA extraction kit (Omega biotek) and the expression of *IFNL1*, *TNF*, and *CXCL10* mRNA was evaluated as described below.

RT-qPCR

mRNA levels of *IFNL1, TNF, CCL2, CXCL10, OAS1* and *OAS3* in human A549 cells; mRNA levels of *CCL2, IL-6, TNF* and *CXCL10* in human PBMCs; viral genomic RNA and viral gene 7 subgenomic (sg) mRNA in human PBMCs; and mRNA levels of *Ccl2, Cxcl10*, *Tnf*, *Ccl8*, and *Oas3* in mice lungs, were analyzed using RNA extracted from cellular extracts. Retrotranscriptase (RT) reactions were performed using the High-Capacity cDNA transcription kit (ThermoFisher Scientific) at 37°C for 2 h, using random primers, and total RNA as template. qPCRs were performed using TaqMan gene expression assays (Applied Biosystems) specific for human *IFNL1* (Hs00601677_g1), *TNF* (Hs00174128_m1), *CXCL10* (Hs00171042_m1), *CCL2* (Hs00234140_m1), *IL6* (Hs 00174131_m1), *OAS1* (Hs00973635_m1), *OAS3* (Hs00196324_m1), *GAPDH* (Hs02786624_g1), and murine *Ccl2* (Mm00441242_m1), *Cxcl10* (Mm00445235_m1), *Tnf* (Mm00443258_m1), *Ccl8* (Mm01297183_m1), *Oas3* (Mm00460944_m1) and *Hprt1* (Mm00446968_m1) genes. Data from qPCR were analyzed following threshold cycle ($2^{-\Delta\Delta CT}$) methodology and normalized with *GAPDH* or *Hprt1* expression levels.

To analyze viral replication and transcription, qPCR was performed using the primers SARS-2-RdRp-15431-VS (5′-GTGAAATGGTCATGTGTGGCGG-3′) and SARS-2RdRp-15530-RS (5′- CAAATGTTAAAAACACTATTAGCATA-3′), complementary to the viral genomic RNA (gRNA)[72]; and the primers, SARS-2-leader-VS: 5′- TCCCAGGTAACAAACCAACCAACT-3′, complementary to the leader sequence; and SARS-2-7a-RS: 5′-AAATGGTGAATTGCCCTCGT-3′, were used to amplify the gene 7 subgenomic (sg) mRNA by qRT-PCR.[73] In these cases, GAPDH was used to normalize the data, amplified using the 5′-TGC CATGGGTGGAATCATATTGGA-3’ (sense) and 5′-TCGGAGTCAACGGATTTGGGTCGT-3 (antisense) primers.

Isolation of peripheral blood mononuclear cells (PBMCs)

We obtained an additional blood sample from seven patients of Hospital Clínic that had previously suffered COVID-19 and participated in our genetic study. Samples were obtained at least 18 months after patients had recovered from COVID-19. Two patients were carriers of rare *OAS1* or *OAS3* variants of interest and the rest were also hospitalized COVID-19 patients devoid of rare *OAS1* or *OAS3* variants. PBMCs were obtained after gradient centrifugation of blood with Ficoll-Paque (GE-Healthcare) at 500 xg for 35 min at room temperature. PBMCs were resuspended in complete culture medium (RPMI 1640-Glutamax, 100 U/mL penicillin, 100 mg/mL streptomycin, 10 mM HEPES, 1 mM sodium pyruvate, 50 mM β-mercaptoethanol, 5% ABS serum) at 10^7 cells/mL and plated in 96 well/plate U bottom at 2×10^6 cells/well.

Generation of human recombinant wild type and mutant OAS1 proteins

We cloned, produced, and purified 2 isoforms of OAS1-p46 in E. coli. Sequences of two isoforms, OAS1-WT and OAS1-K206Q, comprised between residues 1–347 (synthesized by GeneArt, Thermo Fisher Scientific) were cloned in the pGEX-6P-2 plasmid (NovoPro). Constructs were transformed in *E. coli* strain BL21 (DE3) in 2 L of LB medium and protein expression was induced with 0.1 mM IPTG O/N at 16 °C. After centrifugation and PBS wash, pellets were stored at −80°C. For purification, pellets were resuspended in lysis buffer (50 mM Tris-HCl pH 7.4, 300 mM NaCl, 5 mM $MgCl_2$, 10% (vol/vol) glycerol, 0.1 mM EDTA, 2 mM DTT, 1% Triton X-100, with protease inhibitors) and cells were lysed by means of a cell disruptor using Emulsiflex-C3 equipment. The soluble fraction was separated through centrifugation at 15,000 x *g* for 45 min. Column purification was performed using AKTA equipment. We used GST tag affinity chromatography with GSTrap HP column of 1 mL (Cytiva, 17528102). Samples were eluted with isocratic gradient with 100% elution buffer (50 mM Tris-HCl pH 8.0, 300 mM NaCl, 5 mM $MgCl_2$, 10% (vol/vol) glycerol, 0.1 mM EDTA, 2 mM DTT, and 40 mM reduced glutathione). Purification and removal of GST were assessed by 12% SDS-PAGE and protein bands were visualized using TGX and Western blot with an anti-GST antibody (1:1000, clone 8–326, Thermo Fisher Scientific, # MA4-004-HRP, RRID:AB_2537634). The fractions of interest were pooled and dialyzed in 50 mM Tris-HCl pH 7.4, 150 mM NaCl, 1 mM EDTA, 1 mM DTT, pH 7.0. The protein concentration was determined by absorbance at 280 nm. GST was digested with PreScission protease (Cytiva 27084301) following the instructions of the manufacturer. A second purification round was carried out as above. Finally, the samples without GST were subjected to an additional purification step with size exclusion chromatography (SEC). Samples were stored at −20°C in 45 mM Tris-HCl pH7.4, 135 mM NaCl, 0.9 mM DTT and 20% glycerol.

OAS1 enzymatic activity

OAS1 enzymatic activity was studied at Bellbrook Labs by means of an enzyme-coupled method using the AMP the Transcreener AMP^2 Fluorescent Polarization (FP) assay as described (https://www.bellbrooklabs.com/products/transcreener-hts-assays/oas1-assay). The human WT OAS1-p46 protein we generated and one standard WT OAS1-p42 enzyme (Bellbrook) were titrated starting at 150 nM and ending at 0.005 nM (16 points, $n = 2$, 1:2-fold dilution). The OAS1 enzyme carrying the K206Q variant was titrated starting at 2 μM and ending at 0.06 nM (16 points, $n = 2$, 1:2-fold dilutions). Enzymes were titrated in the presence of 5 μg/mL dsRNA and 500 μM ATP, 100 nM coupling enzyme, 16 μg/mL AMP^2/GMP^2 antibody (Bellbrook labs, #2247), 4 nM AMP^2/GMP^2 tracer in 1X OAS1 assay buffer. Using optimal concentration for a 60-min reaction based on data from enzyme titrations, activity was monitored

over a 2-h time course using the same reaction conditions (30°C incubation, readings at 15, 30, 60, 90, and 120 min incubation times). A standard curve mimicking conversion of ATP to AMP was run to allow conversion of FP values to [2-5A] formed for both assays. dsRNA was titrated with each enzyme using the optimal enzyme concentration determined from the titrations with 1 mM ATP, 100 nM coupling enzyme, 16 μg/mL AMP^2/GMP^2 antibody, 4 nM AMP^2/GMP^2 tracer in 1X OAS Buffer. The reaction was run for 60 min at 30°C before being read on the CLARIOstar plus. A standard curve mimicking 100%–0% conversion of 1 mM ATP to AMP was run to allow conversion of FP to [2-5A] formed. Non-linear regression analysis was performed to determine the EC50 concentration. A saturating concentration of dsRNA based on this titration was used for the following experiments. K_M and V_{max} determination was done using saturating dsRNA at ATP concentrations of 2 mM, 1 mM, 500 μM, 250 μM, 100 μM, 50 μM, 25 μM, and 10 μM. Further reaction conditions include 27.5 μg/mL AMP^2/GMP^2 antibody, 4 nM AMP^2/GMP^2 tracer, and 100 nM Coupling Enzyme in 1X OAS1 Buffer. Time vs. AMP (2-5A) was plotted for each ATP concentration. The slopes (velocity) of the Time vs. AMP (2-5A) lines were plotted vs. the ATP concentrations for each enzyme and non-linear regression was performed to obtain K_M and V_{max}.

Intratracheal administration of poly(I:C) and sample processing

Treatment

Under isoflurane anesthesia, mice received intratracheal administration of the immunostimulant agonist of toll-like receptor-3 (TLR-3) poly (I:C). A dose (60 μg in 60 μL of sterile H_2O) was given daily for 4 days. The mice were daily weighted and observed for assessment of any abnormal behavior. At the endpoint, mice were deeply anesthetized and euthanized. Blood was studied in a hematology analyzer (DH36, Dymind Biotechnology). Plasma was obtained for Ccl2 ELISA assay (Invitrogen, # 88–7391). Mice were assigned a code that did not reveal the identity of the samples. Treatment with drug or vehicle was given in a blinded fashion and the treatment was allocated sequentially in an alternate fashion per each experiment.

Lung RNA extraction

We used TrizolVR Reagent (Life Technologies) followed by PureLinkTM RNA Mini Kit (#12183018 A, Invitrogen), and assessed RNA quantity and quality using an ND-1000 micro-spectrophotometer (NanoDrop Technologies). 1 μg total RNA was reverse-transcribed and the final product was diluted six times in RNase-free water. Real-time quantitative RT-PCR analysis was carried out with Taqman system (#4304437, Life Technology) using iCycler iQTM Multicolor Real-Time Detection System (Bio-Rad). The Taqman primers used were: *Ccl2* (Mm00441242_m1); *Tnf* (Mm00443258_m1); *Cxcl10* (Mm00445235_m1); *Ccl8* (Mm01297183_m1); *Oas3* (Mm00460944_m1, and Mm00460945_m1); *Hprt1* (Mm00446968_m1).

Flow cytometry of the lungs

The chest cavity was opened, the left atrium nicked, and the lungs were perfused with 10 mL of heparinized PBS through the right atrium. The right lung was then processed as follows, the lung was immersed in Hanks' Balanced Salt solution w/o ions (HBSS w/o Ca^{2+} and Mg^{2+}; #14175–053, Thermo Fisher Scientific) on ice. Enzymatic dissociation with 100 U/mL collagenase IV and 50 U/mL DNAse I was used to homogenize the tissue. Mechanical dissociation was performed with the gentleMACS Octo Dissociator (#130-096–427, Miltenyi Biotec: 2× Multi c_02_01 program, 1× ABDK_37C program and 1× Multi c_02_01 program). The tissue was then filtered through a 40 μm cell strainer (#352340, Falcon) previously humidified with HBSS with Ca^{2+} and Mg^{2+} (#14025–092, Thermo Fisher Scientific). Unspecific binding of antibodies was blocked by previous incubation for 10 min with anti-CD16/CD32 (Fc block, 1:200, clone 2.4G2, BD Pharmingen, #553145, RRID:AB_394660) together with Live/dead Aqua cell stain (1:1000, Thermo Fisher Scientific, #L34957) to determine the viability of cells. Cells were incubated for 30 min at 4°C with the following primary antibodies: CD11b (1:200, clone M1-70, Brilliant Violet 650, Biolegend, #101239, RRID:AB_11125575), MHCII (IA/IE) (1:400, clone M5/114,15,2, Brilliant Violet 711, Biolegend, #107643, RRID:AB_2565976), CD69 (1:200, clone H1.2F3, FITC, Biolegend, #104506, RRID:AB_313109), Ly6C (1:200, clone HK1.4, PerCP-Cy5.5, Biolegend, #128012, RRID:AB_1659241), CD3 (1:200, clone 17A2, PE, BD BioSciences, #555275, RRID:AB_395699), CD64 (1:200, clone X54-5/7,1, PE/Cy7, Biolegend, #139314, RRID:AB_2563904), CD11c (1:200, clone N418, APC, eBioSciences, #17-0114-82, RRID:AB_469346), Ly6G (1:200, clone 1A8, AF700, Biolegend, #127622, RRID:AB_10643269), CD45 (1:200, clone 30-F11, APC-eFluor 780, eBioSciences, #47-0451-82 RRID:AB_1548781) in Brilliant Violet Stain Buffer (#566349, BD Biosciences), guided by a previous report.[74] The cells were analyzed in a BD Fortessa 5L cytometer using FacsDiva software (version 5, BD Biosciences). Data analyses were performed with FlowJo software (version 10, FlowJo LLC).

In vivo *assessment of lung protein synthesis*

We used the surface sensing of translation (SUnSET), method[75] to assess protein synthesis based on the incorporation of puromycin into nascent lung proteins. Mice received an i.p. administration (100 μL) of puromycin (0.040 μmol/g of body weight) or vehicle (PBS). Thirty min later, mice were perfused with 10 mL of heparinized PBS. The lungs were extracted and immediately frozen in liquid N_2 for Western blotting.[76]

Western blotting

Lung tissue was homogenized in radio-immunoassay precipitation (RIPA) buffer with protease inhibitors (PierceTM, #A32963, Thermo Scientific), centrifuged for 20 min at 12,000 xg at 4 °C and the supernatant was used for protein determination by the Bradford method. Twenty-five μg of protein were mixed with loading buffer containing β-mercaptoethanol and samples were loaded in 10% polyacrylamide gels for electrophoresis. Proteins were then transferred to a polyvinylidene fluoride membranes (Immobilon-P, #IPVH00010, Millipore) and incubated overnight at 4 °C with primary antibodies, followed by horseradish peroxidase-conjugated secondary antibodies, during 1 h at RT. The primary antibody against puromycin (mouse monoclonal, clone 12D10,

Sigma-Aldrich, #MABE343, RRID:AB_2566826) was used diluted 1:500. Anti-GAPDH was used, diluted 1:10,000, for the loading control (Abcam, #ab9484, RRID:AB_307272).

Histological analysis of the lungs

Mice were anesthetized with 5% isoflurane and intracardially perfused with 40 mL heparinized PBS with a perfusion pump at 5 mL/min. Lungs and trachea were dissected out and the trachea was cannulated under a magnifying glass to slowly perfuse paraformaldehyde (PFA) (4%). Lungs are kept in 4% PFA for 12h, washed in PBS, included in paraffin, cut in 5 μm-thick sections in a microtome, and stained with hematoxylin and eosin. Pictures of different lung regions (n = 3) per mouse were obtained and analyzed with ImageJ in a blinded fashion. We determined the percentage of tissue area versus the percentage of alveolar area.

Mouse infection with a mouse-adapted SARS-CoV-2 viral strain

For SARS-CoV-2 infections, Oas3$^{-/-}$ and Oas3$^{+/+}$ mice bred at the UB vivarium were sent to the biosafety level 3 (BSL3) animal facilities in the Animal Health Research Center (CISA-INIA, CSIC) in Madrid (Spain), where the mice stayed in pathogen-free conditions, one week before mice inoculation. Male mice at the ages of 2.5–4.5-month-old were slightly anesthetized with isoflurane and then, intranasally inoculated with 5,000 FFU/mice of a mouse-adapted SARS-CoV-2-MA strain (see above under 'Viruses' heading). We excluded mice that showed no evidence of infection (no body weight loss or lack of viral titers in the lung) due to unsuccessful viral administration. Mice of each genotype received treatment in parallel, but genotype could not be blinded due to the logistic complexity of BSL3 facilities. Mice (n = 17/group) were examined each day for weight loss, clinical symptoms (such as malaise, respiratory distress, and lack of movement) and mortality up to day 10 post-infection. Percent body weight loss was determined relative to the starting weight. Mice that lost more than 25% of their initial body weight were considered to have reached the experimental endpoint and were humanely euthanized. These mice were classified as non-survivors. Two mice out of the 17 from each group Oas3$^{+/+}$ and Oas3$^{-/-}$ were excluded from the analysis as they did not lose any weight.

Virus replication was evaluated in other groups of mice by assessing viral titers in the lungs at 4 dpi (n = 12 and 15 for Oas3$^{+/+}$ and Oas3$^{-/-}$, respectively), or 2 dpi (n = 4 per group). From the Oas3$^{+/}$ group to be studied at 4 dpi (n = 12 mice), we had to exclude five mice; two of them showed no viral titers in the lungs and three other mice fought among them, getting severely injured. Furthermore, one mouse of the 4 dpi Oas3$^{-/-}$ group (n = 15) died before the endpoint and we could not extract its organs. Mice were euthanized, and the right lung lobules were extracted in 1 mL of PBS and one 5 mm stainless steel bead (Qiagen) and homogenized using the TissueLyser II (Qiagen) at 25 Hz for 5 min, followed by centrifugation at 5,000 x g for 10 min at 4°C. Virus titers were determined by a plaque titration assay on Vero-TMPRSS2 cells as specified above. In these same mice, levels of *Oas3, Ccl2, Cxcl10* and *Tnf* induction were analyzed by RT-qPCR in lungs at 2 and 4 dpi. To this end, the left lung lobules were extracted and incubated in RNAlater (Ambion) at 4°C for 24 h prior to adding the lungs to RNA lysis buffer and one 5 mm stainless steel bead (Qiagen). The samples were homogenized using the TissueLyser II (Qiagen) at 25 Hz for 5 min, and total RNA was extracted from homogenized lungs using the total RNA kit (Omega Biotech). RT-qPCR reactions were performed as described above. Sera from mock-infected and infected mice were collected at 4 dpi and diluted 1:2 in assay buffer (Millipore) before analysis. The expression of Tnf, Ccl2/Mcp-1, Cxcl2, Ccl5/Rantes, and Cxcl10/IP-10 was measured using Luminex technology and a mouse cytokine antibody bead kit (Milliplex map kit; Millipore) according to the manufacturer's instructions.

QUANTIFICATION AND STATISTICAL ANALYSIS

Power analysis for the human studies

We assessed the sample size to detect meaningful differences among the three clinical groups (ICU patients, non-ICU hospitalized patients, and non-hospitalized individuals) by conducting a statistical power analysis using a chi-square goodness-of-fit test. The total cohort comprised 342 individuals (61 ICU, 199 non-ICU hospitalized, and 82 non-hospitalized). We evaluated the power of the study to detect small (Cohen's w = 0.1), moderate (w = 0.3), and large (w = 0.5) effect sizes, using a significance level of $\alpha = 0.05$ and three outcome categories. The results showed that the study had:

36.1% power to detect a small effect size, 99.9% power to detect a moderate effect size, and >99.999% power to detect a large effect size.

These calculations were performed using the GofChisquarePower class from the statsmodels Python package, specifying the number of bins as 3. The choice of a moderate effect size as a reference is grounded in the typical expectations for genetic association studies involving complex traits, where moderate effects are often considered biologically relevant and statistically detectable in well-powered cohorts. Therefore, our sample size is robust and adequately powered to detect moderate to large differences across clinical groups but no small effects.

Regression analysis

All analyses were performed using Python version 3.13, leveraging the *pandas* library for data manipulation, the *statsmodels* library for regression modeling and the *matplotlib* and *seaborn* libraries for data visualization. A p-value of less than 0.05 was considered statistically significant for all tests.

Predictor variables were presence of rare variants, age, sex, ethnicity and genotype at rs10774671. Ethnicity was coded in three categories: European origin, Latin-American origin and Other, grouping African, South-East Asian and East Asian. Severity was the

dependent variable with two (non-hospitalized and hospitalized) or three (non-hospitalized, hospitalized without ICU admission and hospitalized with ICU admission) categories.

In the multivariate analysis, with three categories in the Severity term, we first determined the independent contribution of each predictor. Then, we explored the possible interaction between age and presence of rare variants.

In the binary logistic regression analysis, the dependent variable consisted of two categories, non-hospitalized and hospitalized that was formed by all hospitalized patients regardless of ICU admission. Then we look for the independent contribution of each predictor on the odds of hospitalization followed by the fitting of a model that included the main effects plus an interaction term between age and presence of a rare variant.

In this latter analysis, absence of significant multicollinearity was assessed calculating the variance effect interaction (VEI) for each term in the main effects model, considering VIF<5 as the threshold marking a stable model.

In both analysis we only tested the interaction between age and the presence of rare variants as there were a significant loss in statistical power when trying to analyze other interactions due to the small size of the groups.

Analysis pipeline

Demultiplexing was accomplished using bcl2fastq2 v2.20.0.422 (Illumina Inc.). Quality control of reads was done using FastQC v0.11.9 (http://www.bioinformatics.babraham.ac.uk/projects/fastqc/) and MultiQC v1.13 (https://multiqc.info/ and Ewels et al.[77]). Alignment against the human genome (hg19 built) with BWA-MEM 0.7.17 (https://github.com/bwa-mem2/bwa-mem2) and for variant calling we used GATK 4.0.3.0 (https://gatk.broadinstitute.org/hc/en-us). Variants were then filtered by selecting those with a depth over 20x and a genome quality score over 20. Finally, variant annotation was done VEP and pathogenicity prediction was done using REVEL implemented in VEP (https://www.ensembl.org/info/docs/tools/vep/index.html and Ioannidis et al.[78]), and SIFT (https://sift.bii.a-star.edu.sg/index.html and Ng and Henikoff[79]), PolyPhen2 (http://genetics.bwh.harvard.edu/pph2/index.shtml and Adzhubei et al.[80]), CADD (https://cadd.gs.washington.edu/ and Kircher et al.[81]) and MutationTaster.[67] The analysis pipeline can be found at https://doi.org/10.5281/zenodo.17396248.

Gene-based association analysis

Ultra-rare variants were pooled together and compared between groups. The variants were grouped by gene but also, due to the close vicinity of *OAS1* and *OAS3* in the same *locus*, grouping those in *OAS1* and *OAS3* together. We did not include *OAS2* as there were no potential pathogenic variants in this gene in the Spanish cohort and it is in the telomeric part of the *locus*. For this analysis we used the optimal sequence kernel association test (SKAT-O) (41) using the R-package SKAT.

Analysis of rs10774671

Univariate analysis of rs10774671 with severity was done using the chi-square of exact Fisher test as appropriate using R. Hardy-Weinberg equilibrium was tested with the HardyWeinberg R package (version 1.7.8).

To test the influence of this polymorphism in severity we used R (version 4.1.2) and the SKAT package (version 2.2.5). The genotype matrix was built so that homozygous reference, heterozygous, and homozygous alternative genotypes were assigned a value of 0, 0.5 and 1, respectively. The categorical phenotypic data were converted into numeric factors. A null model was constructed incorporating haplotypic information (rs10774671 genotype) as a covariate. SKAT analysis was performed using both the optimal adjustment and the common-rare variant methods. The heatmap was generated using the heatmap package (version 1.0.12). This analysis was done by EGO Genomics SL (Villamayor, Spain).

Statistical methods for animal studies

Two-group comparisons were carried out with a two-tailed Mann–Whitney test or *t* test, as required after testing for normality. Multiple groups were compared with one-way or two-way ANOVA, followed by appropriate post hoc analyses. Survival curves were compared with the Log rank (Mantel-Cox) test. Specific tests used in each experiment, *p*-values, and *n* values are stated in the figure legends. We estimated the required sample sizes in mouse experiments using G*Power 3.1.9.4. For the viral infection study, we assumed an effect size of 0.9, an alpha error probability of 0.05, and a statistical power of 0.8, which yielded a required sample size of approximately 16 mice per group. For the poly(I:C)-induced inflammation study, we assumed a larger effect size of 1.5 based on prior *in vitro* data showing substantially higher inflammatory responses in the $Oas3^{-/-}$ genotype. Using the same alpha level and power, this yielded a required sample size of approximately 7 mice per group. Values are expressed as the mean ± SD. We used GraphPad Prism software version 9.3.1.